repiSalud
Repositorio Institucional en Salud

This is the peer reviewed version of the following article:

Desdin-Mico, G., Soto-Heredero, G., Aranda, J. F., Oller, J., Carrasco, E., Gabande-Rodriguez, E., . . . Mittelbrunn, M. (2020). T cells with dysfunctional mitochondria induce multimorbidity and premature senescence. *Science, 368*(6497), 1371-1376. doi:10.1126/science.aax0860

which has been published in final form at: https://doi.org/10.1126/science.aax0860

Immunometabolic T cell failure induces multimorbidity and aging

Gabriela Desdín-Micó[1,2], Gonzalo Soto-Heredero[1,2†], Juan Francisco Aranda[1,2†], Jorge Oller[1,2†], Elisa Carrasco[1,2], Enrique Gabandé-Rodríguez[1,2], Eva Maria Blanco[1,2], Arantzazu Alfranca[3], Lorena Cusso[4,5], Manuel Desco[4,5], Borja Ibañez[5,6,7], Arancha R. Gortazar[8], Pablo Fernández-Marcos[9], Maria N. Navarro[2,3], Bruno Hernaez[2], Antonio Alcamí[2], Francesc Baixauli[10¶]

and María Mittelbrunn[1,2 ¶*]

Affiliations:

[1]Instituto de Investigación Sanitaria Hospital 12 de Octubre (imas12), Madrid, Spain
[2]Departamento de Biología Molecular, Centro de Biología Molecular Severo Ochoa (CBMSO), Consejo Superior de Investigaciones Científicas (CSIC)-Universidad Autónoma de Madrid (UAM), Madrid, Spain
[3]Hospital Universitario de la Princesa, Madrid, Spain
[4]Departamento de Bioingeniería e Ingeniería Aeroespacial, Universidad Carlos III de Madrid, Instituto de Investigación Sanitaria Gregorio Marañón; Centro de Investigación Biomédica en Red de Salud Mental (CIBERSAM), Spain
[5]Centro Nacional de Investigaciones Cardiovasculares (CNIC), Madrid, Spain
[6]IIS-Fundación Jiménez Díaz, Madrid, Spain
[7]CIBERCV, Madrid, Spain, Madrid, Spain
[8]Bone Physiopathology Laboratory, Applied Molecular Medicine Institute (IMMA), Universidad San Pablo-CEU, Madrid, Spain
[9]Metabolic Syndrome Group - BIOPROMET, Madrid Institute for Advanced Studies - IMDEA Food, CEI UAM+CSIC, Madrid, Spain
[10]Department of Immunometabolism, Max Planck Institute of Immunobiology and Epigenetics, Freiburg, Germany

*Correspondence to: mmittelbrunn@cbm.csic.es

†¶ for equal contributions

One Sentence Summary: T cell metabolic stress induces systemic aging.

Abstract:

The impact of immunometabolism on age-associated diseases remains uncertain. Here, we show that T cells with dysfunctional mitochondria act as aging accelerators. They instigate multiple age-related features, including metabolic, cognitive, physical and cardiovascular alterations, which together result in premature death. Metabolic failure in T cells induces the accumulation of circulating cytokines, resembling the chronic inflammation that characterizes aging ("inflammaging"). We also present evidence that this cytokine storm is a systemic inducer of senescence. Dampening inflammation by blocking TNF-α signaling or preventing senescence with NAD^+ precursors partially rescue premature aging in mice with metabolically defective T cells. Thus, T cells have the capacity to regulate organismal fitness and lifespan, highlighting the importance of tight immunometabolic control in both aging and the onset of age-associated diseases.

Main text:

The emerging field of immunometabolism (*1-5*) is opening up therapeutic opportunities for the treatment not only of inflammatory and autoimmune disorders (*6*), but also of metabolic diseases and cancer (*7-10*). However, the utility of targeting immunometabolism to prevent the onset of age-associated diseases and multimorbidity has not been previously addressed.

An age-related decline in mitochondrial function has been observed in various cells and tissues, including T cells (*11*). To investigate the consequences of T cell metabolic decline in healthy aging, we used $Tfam^{fl/fl}\ Cd4^{Cre}$ mice. *Tfam* is a nuclear gene encoding mitochondrial transcription factor A (TFAM), which both stabilizes mtDNA and initiates mtDNA replication (*12*). In $Tfam^{fl/fl}\ Cd4^{Cre}$ mice, Tfam is depleted in both CD4 and CD8 T lymphocytes (*13*). Lack of Tfam in T cells reduced the numbers of total circulating CD4 and CD8 T cells (fig. S1A). Tfam depletion induced a sharp decrease in their mtDNA content (fig. S1B) and the loss of expression of key electron transport chain components, forcing a metabolic reprogramming towards glycolysis (*13*) (Fig. 1A-C). T cells from young (2 months old) $Tfam^{fl/fl}\ Cd4^{Cre}$ mice recapitulated features of the mitochondrial dysfunction that appears in aged (22 months old) wild-type mice (Fig. 1A-C). This mitochondrial decline was associated with Th1 cell skewing, characterized by higher secretion of inflammatory type 1 cytokines IFN-γ and TNF-α, and the increased expression of the Th1 cell master regulator

T-bet (Fig. 1D-E, fig. S1C). In addition to this pro-inflammatory phenotype, young (2 months old) *Tfam*$^{fl/fl}$ *Cd4*^{Cre} mice were immunocompromised to a similar extent as old (22 months old) wild-types. We infected *Tfam*$^{fl/fl}$ *Cd4*^{Cre} mice with ectromelia virus (ECTV), a highly virulent mouse poxvirus that causes a disease similar to human smallpox, and compared them with young or old control mice. Infection with ECTV killed old wild type mice and young *Tfam*$^{fl/fl}$ *Cd4*^{Cre} mice in the first 10 days of infection, whereas all young controls were able to survive this acute infection (Fig. 1F). Thus, *Tfam*-deficient T cells recapitulate metabolic, phenotypic and functional features of aged T cells. We observed that *Tfam*$^{fl/fl}$ *Cd4*^{Cre} mice presented premature inflammaging, with 7-month-old *Tfam*$^{fl/fl}$ *Cd4*^{Cre} mice having similar serum levels of the inflammaging-associated cytokines IL-6, IFN-γ, and TNF-α to 22-month-old wild types (Fig. 1G, fig. S1D-E). In humans, inflammaging predicts susceptibility to cardiovascular diseases, neurodegeneration, frailty, and multimorbidity (*14-16*). *Tfam*$^{fl/fl}$ *Cd4*^{Cre} mice displayed a premature aged appearance from the age of 7 months (Fig. 1H) and developed anemia, kyphosis, and low body weight (Fig. 1I-K, fig. S1F). An additional indicator of aging in *Tfam*$^{fl/fl}$ *Cd4*^{Cre} mice was a significant thinning of hypodermal fat (Fig. 1L). Consistent with a premature aging phenotype, metabolic cage experiments revealed that *Tfam*$^{fl/fl}$ *Cd4*^{Cre} mice were less active and slower than controls, despite higher energy expenditure (Fig. 1M, fig. S1G). Importantly, mean lifespan in *Tfam*$^{fl/fl}$ *Cd4*^{Cre} mice was half that of controls (483 days versus 984 days) (Fig. 1N). Although Tfam deletion in regulatory T cells induces lethal autoimmunity (*17*), *Tfam*$^{fl/fl}$ *Cd4*^{Cre} mice showed no differences in the level of serum autoantibodies (fig. S1H).

To evaluate the potential of *Tfam*$^{fl/fl}$ *Cd4*^{Cre} mice as a model of age-related multimorbidity, we analyzed muscular, cardiovascular, and cognitive fitness. Histological analyses of *Tfam*$^{fl/fl}$ *Cd4*^{Cre} muscle revealed a reduced fiber diameter (Fig. 2A). Imaging analysis of gastrocnemius muscle after injection of ^{18}F-fluorodeoxyglucose (^{18}F-FDG) revealed significantly lower glucose uptake in *Tfam*$^{fl/fl}$ *Cd4*^{Cre} mice (Fig. 2B). Lower skeletal muscle strength was confirmed by the grip strength test (Fig. 2C). Moreover, *Tfam*$^{fl/fl}$ *Cd4*^{Cre} muscle upregulated the expression of genes encoding the ubiquitin ligases MuRF-1 and Atrogin-1, as well as inflammatory markers (Fig. 2D, fig. S2A). *Tfam*$^{fl/fl}$ *Cd4*^{Cre} mice displayed a marked loss of gWAT mass, and smaller adipocytes (Fig. 2E,F). These differences were accompanied by elevated expression levels of the adipose triglyceride lipase (ATGL) and plasma levels of non-esterified fatty acids in *Tfam*$^{fl/fl}$ *Cd4*^{Cre}, indicating lipolysis induction (Fig. 2G,H). Thus, the loss of T cell immunometabolic control induces sarcopenia and

lipolysis. *Tfam*$^{fl/fl}$ *Cd4*^{Cre} mice showed evidence of cardiac atrophy (Fig. 2I, fig. S2B). Histological and echocardiographic analysis revealed relative reduction in left ventricular thickness, reduced left ventricular diameter and volume, and smaller cardiomyocyte size (Fig. 2J, fig. S2C-F). These features were accompanied by a higher heart rate (Fig. 2K) and the induction of cardiac stress markers *Foxo3a* and *Nppa* (fig. S2G). *Tfam*$^{fl/fl}$ *Cd4*^{Cre} mice displayed diastolic failure characterized by reduced cardiac output, as well as elevated normalized lung weight together with signs of lung congestion on CT scan (Fig. 2L,M, and fig. S2H). Diastolic dysfunction was also evident from left ventricular (LV) relaxation defects detected in the mitral flow pattern (Fig. 2N). *Tfam*$^{fl/fl}$ *Cd4*^{Cre} mice developed an age-dependent aortic dilation (Fig. 2O) correlated with increased mRNA expression of inducible nitric oxide synthase (*Nos2*), decreased mRNA expression of the contractile markers as well as decreased blood pressure (Fig. 2P,Q). Consistent with these findings, 77% of *Tfam*$^{fl/fl}$ *Cd4*^{Cre} mice had aortic regurgitation, compared with 16% of controls. Histological analysis of the aortas allowed us to identify aortic dissections associated with inflammatory foci in 50% of *Tfam*$^{fl/fl}$ *Cd4*^{Cre} animals (fig. S2I). Thus *Tfam*$^{fl/fl}$ *Cd4*^{Cre} mice appear to develop cardiac atrophy and overt heart failure, and severe cardiovascular alterations, which can precipitate death. *Tfam*$^{fl/fl}$ *Cd4*^{Cre} mice also showed signs of neurological disability, including an influx of T cells in the fornix area of the brain and defects in motor coordination in both the rotarod and the tail suspension tests (Fig. 2R-T). Together, these data support a role for T cells beyond host defense (*18, 19*), and indicate that the metabolic fitness of T cells is critical for organismal homeostasis.

To verify whether this multimorbidity phenotype was due to a mitochondrial failure in T cells, we used an alternative to delete *Tfam* in T cells. We generated *Tfam*$^{fl/fl}$ *Lck*^{Cre} mice, in which Cre recombinase is expressed under the control of the lymphocyte protein tyrosine kinase (Lck) promoter. *Tfam*$^{fl/fl}$ *Lck*^{Cre} mice presented comparable metabolic and functional alterations in T cells, and similar premature age-associated multimorbidity to *Tfam*$^{fl/fl}$ *Cd4*^{Cre} mice (fig. S3). To identify the molecular mechanism by which T cell metabolic failure drives organismal frailty and multimorbidity, we performed liver transcriptomics. *Tfam*$^{fl/fl}$ *Cd4*^{Cre} liver showed significant upregulation of genes associated with senescence (fig. S4A). One of the most upregulated transcripts related to senescence was *Cdkn1a*, which encodes the cyclin inhibitor p21 (q-value = 0.003) (Fig. 3A). *Tfam*$^{fl/fl}$ *Cd4*^{Cre} mice showed elevated protein levels of senescence markers p21$^{Waf/Cip1}$ and p53 in the liver. This elevation of p21 was also observed in the heart, gWAT, and pancreas (Fig. 3B). In addition, activity of senescence-associated β-galactosidase was higher in

Tfam$^{fl/fl}$ Cd4^{Cre} gWAT and kidney than in controls (Fig. 3C,D, fig. S4B,C). Analysis of *Tfam$^{fl/fl}$ Lck^{Cre}* mice confirmed senescence induction in various tissues (fig. S3M).

Because in vitro incubation of cancer cells with the type 1 cytokines induces senescence (*20*), we hypothesized that the type 1 cytokines present in *Tfam$^{fl/fl}$ Cd4^{Cre}* mice drive systemic senescence. Incubation of mouse cells with *Tfam$^{fl/fl}$ Cd4^{Cre}* serum or TNF-α was sufficient to increase p21$^{Waf/Cip1}$ levels in hepatocytes, and pre-adipocytes, supporting the argument that inflammatory mediators induce senescence and premature aging (Fig. 3E, fig. S4D). To dissect the contribution of TNF-α to the multimorbidity phenotype, we treated *Tfam$^{fl/fl}$ Cd4^{Cre}* mice with the TNF-α inhibitor etanercept. Blocking TNF-α prevented systemic senescence (Fig. 3F,G) and muscle, cardiovascular and cognitive alterations (Fig. 3H-K). Bone marrow (BM) transplantation from *Tfam$^{fl/fl}$ Cd4^{Cre}* mice into T cell-deficient mice (*Cd3e$^{-/-}$*) (fig. S5A,B) recapitulated the type 1 cytokine storm observed in *Tfam$^{fl/fl}$ Cd4^{Cre}* mice (fig. S5C-E) and showed sings of senescence in multiple tissues (Fig. 3L-N). *Cd3e$^{-/-}$* mice reconstituted with *Tfam$^{fl/fl}$ Cd4^{Cre}* BM, but not with control BM, developed a premature aged appearance after 16 weeks (fig. S5F), and reproduced the multimorbidity phenotype (fig. S5G-J). Thus, T cells with mitochondrial dysfunction are able to induce systemic senescence in peripheral tissues via type 1 cytokine storm.

Notably, the senescence observed in *Tfam$^{fl/fl}$ Cd4^{Cre}* mice was accompanied by a low NAD$^+$/NADH ratio in peripheral tissues (Fig. 4A, fig. S6A). This was consistent with the reported decline in NAD$^+$ levels during aging (*21*). NAD$^+$ is a metabolic cofactor with a critical role in mitochondrial function, and restoring NAD$^+$ levels confers protection against age-associated diseases (*21-25*). Recent data support that supplementation with the NAD$^+$ precursor nicotinamide riboside (NR) reduces inflammaging in the elderly (*26*). Accordingly, we observed that NR decreased the serum levels of TNF-α in aged mice (fig. S6B). To test whether NAD$^+$ boosting strategies could prevent tissue damage caused by inflammaging, we treated *Tfam$^{fl/fl}$ Cd4^{Cre}* mice with NR for 10 weeks to restore the NAD$^+$/NADH ratio (Fig. 4A,B). Although NR neither restored weight loss nor reversed the Th1 cell phenotype (Fig. 4C), it successfully reversed skeletal muscle wasting and anemia. Furthermore, most of the cardiovascular alterations found in *Tfam$^{fl/fl}$ Cd4^{Cre}* mice were also reversed (Fig. 4D-G). NR treatment also increased physical activity levels of *Tfam$^{fl/fl}$ Cd4^{Cre}* mice and reversed tissue senescence and inflammation (Fig. 4H-K, and fig. S6C). Finally, a principal component analysis of liver transcriptomics classified *Tfam$^{fl/fl}$ Cd4^{Cre}* mice treated with NR closer

to controls than to untreated *Tfam*$^{fl/fl}$ *Cd4*^{Cre} mice (Fig. 4L). IPA analysis linked NR treatment to of pathways associated with lipid metabolism, inflammation, morbidity, and mortality (Fig. 4M and table S1). Thus, NR can reverse transcriptional changes related to aging in *Tfam*$^{fl/fl}$ *Cd4*^{Cre} mice.

With the continuous extension of life expectancy, there is an urgent need to understand the common molecular pathways by which aging results in a progressively higher susceptibility to diseases (*27*). Our results indicate that metabolic changes in the immune system promote age-related deterioration in other tissues, leading to multimorbidity and premature death. Dysregulated T cell metabolism triggers a type 1 cytokine storm that induces senescence in several tissues. Furthermore, we have used this novel model of multimorbidity and premature aging to test for drugs that can delay aging signs. We found that NAD^+ precursors can prevent tissue damage associated with sustained inflammation, supporting their potential for preventing age-associated multimorbidity. Whether targeting senescence or boosting NAD^+ levels would have beneficial effects beyond age-associated diseases in patients with cachexia or cytokine-release syndrome will require further investigation. Our results place immunometabolism at the crossroads of inflammation, senescence and aging, highlighting its potential as a therapeutic target for delaying aging and aging-associated diseases.

Reference and Notes:

1. T. N. Tarasenko *et al.*, Cytochrome c Oxidase Activity Is a Metabolic Checkpoint that Regulates Cell Fate Decisions During T Cell Activation and Differentiation. *Cell metabolism* **25**, 1254-1268 e1257 (2017).
2. S. E. Weinberg *et al.*, Mitochondrial complex III is essential for suppressive function of regulatory T cells. *Nature*, (2019).
3. L. A. Sena *et al.*, Mitochondria are required for antigen-specific T cell activation through reactive oxygen species signaling. *Immunity* **38**, 225-236 (2013).
4. E. L. Pearce *et al.*, Enhancing CD8 T-cell memory by modulating fatty acid metabolism. *Nature* **460**, 103-107 (2009).
5. E. L. Mills, B. Kelly, L. A. J. O'Neill, Mitochondria are the powerhouses of immunity. *Nat Immunol* **18**, 488-498 (2017).
6. J. P. Rhoads, A. S. Major, J. C. Rathmell, Fine tuning of immunometabolism for the treatment of rheumatic diseases. *Nat Rev Rheumatol* **13**, 313-320 (2017).
7. C. H. Chang, E. L. Pearce, Emerging concepts of T cell metabolism as a target of immunotherapy. *Nat Immunol* **17**, 364-368 (2016).
8. L. Li *et al.*, TLR8-Mediated Metabolic Control of Human Treg Function: A Mechanistic Target for Cancer Immunotherapy. *Cell metabolism*, (2018).
9. G. S. Hotamisligil, Foundations of Immunometabolism and Implications for Metabolic Health and Disease. *Immunity* **47**, 406-420 (2017).
10. A. Wang, H. H. Luan, R. Medzhitov, An evolutionary perspective on immunometabolism. *Science* **363**, (2019).
11. N. Ron-Harel *et al.*, Defective respiration and one-carbon metabolism contribute to impaired naive T cell activation in aged mice. *Proc Natl Acad Sci U S A* **115**, 13347-13352 (2018).
12. M. I. Ekstrand *et al.*, Mitochondrial transcription factor A regulates mtDNA copy number in mammals. *Hum Mol Genet* **13**, 935-944 (2004).
13. F. Baixauli *et al.*, Mitochondrial Respiration Controls Lysosomal Function during Inflammatory T Cell Responses. *Cell metabolism* **22**, 485-498 (2015).
14. L. Ferrucci, E. Fabbri, Inflammageing: chronic inflammation in ageing, cardiovascular disease, and frailty. *Nat Rev Cardiol* **15**, 505-522 (2018).
15. C. Franceschi, P. Garagnani, P. Parini, C. Giuliani, A. Santoro, Inflammaging: a new immune-metabolic viewpoint for age-related diseases. *Nat Rev Endocrinol* **14**, 576-590 (2018).
16. D. Furman *et al.*, Chronic inflammation in the etiology of disease across the life span. *Nat Med* **25**, 1822-1832 (2019).
17. N. M. Chapman *et al.*, mTOR coordinates transcriptional programs and mitochondrial metabolism of activated Treg subsets to protect tissue homeostasis. *Nat Commun* **9**, 2095 (2018).
18. S. He *et al.*, Gut intraepithelial T cells calibrate metabolism and accelerate cardiovascular disease. *Nature*, (2019).
19. L. C. Rankin, D. Artis, Beyond Host Defense: Emerging Functions of the Immune System in Regulating Complex Tissue Physiology. *Cell* **173**, 554-567 (2018).
20. H. Braumuller *et al.*, T-helper-1-cell cytokines drive cancer into senescence. *Nature* **494**, 361-365 (2013).
21. A. P. Gomes *et al.*, Declining NAD(+) induces a pseudohypoxic state disrupting nuclear-mitochondrial communication during aging. *Cell* **155**, 1624-1638 (2013).
22. E. Verdin, NAD(+) in aging, metabolism, and neurodegeneration. *Science* **350**, 1208-1213 (2015).
23. H. Zhang *et al.*, NAD(+) repletion improves mitochondrial and stem cell function and enhances life span in mice. *Science* **352**, 1436-1443 (2016).
24. E. Katsyuba *et al.*, De novo NAD(+) synthesis enhances mitochondrial function and improves health. *Nature* **563**, 354-359 (2018).
25. S. J. Mitchell *et al.*, Nicotinamide Improves Aspects of Healthspan, but Not Lifespan, in Mice. *Cell metabolism* **27**, 667-676 e664 (2018).
26. Y. S. Elhassan *et al.*, Nicotinamide Riboside Augments the Aged Human Skeletal Muscle NAD(+) Metabolome and Induces Transcriptomic and Anti-inflammatory Signatures. *Cell Rep* **28**, 1717-1728 e1716 (2019).
27. I. Bellantuono, Find drugs that delay many diseases of old age. *Nature* **554**, 293-295 (2018).
28. P. P. Lee *et al.*, A critical role for Dnmt1 and DNA methylation in T cell development, function, and survival. *Immunity* **15**, 763-774 (2001).

29. S. Sawada, J. D. Scarborough, N. Killeen, D. R. Littman, A lineage-specific transcriptional silencer regulates CD4 gene expression during T lymphocyte development. *Cell* **77**, 917-929 (1994).
30. T. Hennet, F. K. Hagen, L. A. Tabak, J. D. Marth, T-cell-specific deletion of a polypeptide N-acetylgalactosaminyl-transferase gene by site-directed recombination. *Proc Natl Acad Sci U S A* **92**, 12070-12074 (1995).

Acknowledgments: We thank N.G. Larsson for *Tfam*$^{fl/fl}$ mice, R. Tejedor and J.L de Pablos for technical support, and C. López-Otín, M. Serrano, and B. Alarcón for scientific discussion. We also thank A. de Francisco, Y. Sierra, and M. de la Jara Felipe for their excellent work with animal preparation and imaging protocols and D. Calle for her help with data processing. **Funding:** This study was supported by the Fondo de Investigación Sanitaria del Instituto de Salud Carlos III (PI16/188, PI19/855), the European Regional Development Fund (ERDF), and the European Commission through H2020-EU.1.1 and European Research Council grant ERC-2016-StG 715322-EndoMitTalk. This work was partially supported by Comunidad de Madrid (S2017/BMD-3867 RENIM-CM). M.M. is supported by the Miguel Servet Program (CP 19/014). G.S.-H. is supported by FPI-UAM, J.O (FJCI-2017-33855) and E.G-R (IJC2018-036850) by Juan de la Cierva, and E.C. by Atracción de Talento Investigador 2017-T2/BMD-5766 (Comunidad de Madrid and UAM). **Author contributions:** G.D-M, G.S-H, J.F.A, J.O, E.C, E.G-R, M.N, L.C, F.B, E.M.B, and B.H. performed experimental work and analyzed the data. B.I, A. Alfranca, M.D. and A. Alcami provided technical and scientific support. F.B. and M.M. designed the research. G.D-M and M.M. wrote the manuscript. G.S-H, J.F.A. and J.O. contributed equally to this study. F.B. and M.M. contributed equally to this study. **Competing interests:** The authors declare no competing interests. **Data and materials availability:** All data are presented in the main text or the supplementary materials.

Supplementary Materials:

Materials and Methods

Figures S1-S6

Table S1

References (28-30)

Fig. 1. ***Mitochondrial dysfunction in T cells causes premature aging***.

(**A**) *Tfam*, *mtCo1* and *mtNd1* mRNA levels in peripheral blood $CD4^+$ T cells from young (2-month-old) $Tfam^{fl/fl}$ and $Tfam^{fl/fl}$ $Cd4^{Cre}$ mice, and old (22-month-old) wt mice (n = 6-9 mice per group). (**B**) Oxygen consumption rates (OCR) in activated $CD4^+$ T cells from $Tfam^{fl/fl}$, $Tfam^{fl/fl}$ $Cd4^{Cre}$ and old wt animals (left). Basal respiration (center) and maximal respiratory capacity (right) are shown (n = 3-4). (**C**) Lactate content in the supernatant of activated $CD4^+$ T cells (n = 3-4). (**D**) Percentages of $CD4^+$ (left) and $CD8^+$ (right) T cells positive for the Th1 cell transcription factor T-bet (n = 5-14). (**E**) Percentages of $CD4^+CD44^{hi}$ T cells staining positive for intracellular IFN-γ and TNF-α (n = 3-9). (**F**) Post-infection survival curves (left panel) for $Tfam^{fl/fl}$, $Tfam^{fl/fl}$ $Cd4^{Cre}$ and old wt mice inoculated s.c. with ECTV (10^3 PFUs per mouse). ECTV-infected mice were monitored daily for clinical signs of illness (center) and change from initial body weight (right). Signs of illness are expressed as means ± SEM using an individual score ranging from 0 for healthy animals to 4 for severely diseased animals (n = 5-7). (**G**) Serum levels of inflammatory cytokines IL-6 and TNF-α detected by Multiplex in 7-month-old $Tfam^{fl/fl}$ and $Tfam^{fl/fl}$ $Cd4^{Cre}$ mice and 22-month-old wt mice (n = 10-19). (**H**) Representative photograph showing the deteriorated physical appearance of a $Tfam^{fl/fl}$ $Cd4^{Cre}$ mouse (right) compared with a control littermate (left), both aged 7 months. (**I**) Hematological parameters in $Tfam^{fl/fl}$ $Cd4^{Cre}$ and $Tfam^{fl/fl}$ mice (n = 8-11, 5 months old). (**J**) Quantification of spine curvature by computed tomography (CT) scans (left) and percentage of mice presenting lordokyphosis (right) in 5-month-old $Tfam^{fl/fl}$ $Cd4^{Cre}$ mice (n = 7-8). (**K**) Body weight evolution in $Tfam^{fl/fl}$ and $Tfam^{fl/fl}$ $Cd4^{Cre}$ female (left) and male (right) mice (n = 8-20). (**L**) Representative skin sections stained with Masson trichrome (left) and quantification of hypodermal fat thickness (right). At least 10 measurements were performed per animal. The graph shows mean values for n = 7, 7 months of age. Scale bar: 100 μm. (**M**) Activity time course over a 24-hour cycle (left) and mean dark period activity (center) and speed (right) assessed in metabolic cages (n = 6-9, 7-month-old mice). Bar graphs correspond to the dark (active) period. (**N**) Kaplan–Meier survival curves for $Tfam^{fl/fl}$ and $Tfam^{fl/fl}$ $Cd4^{Cre}$ mice (n = 36-38, including males and females). Dots in all panels represent individual sample data. Data are presented as means ± SEM. Statistical analysis was by one-way analysis of variance (ANOVA) with post hoc Tukey's correction [**A** (*mtCo1* and *mtNd1*), **C**, **D** and **G** (TNF-α)]; Kruskal–Wallis *H* test with post hoc Dunn's correction [**A** (*Tfam*), **B** and **G** (IL-6)], unpaired Student's *t*-test [**I** (MCV), **J**, **K** and **M**]; or unpaired Welch's *t*-test [**L** and **I** (Hemoglobin)]. *p<0.05, **p<0.01, ***p<0.001, ****p<0.0001. Survival curve data were analyzed by log-rank (Mantel–Cox test) [**F** and **N**]. For the ECTV experiment, data correspond to one representative experiment of two.

Fig. 2. ***Tfam$^{fl/fl}$ Cd4^{Cre} mice develop age-associated multimorbidity.***

(A) Representative haematoxylin and eosin (H&E)–stained sections of gastrocnemius muscle (left, scale bar: 50 μm) and quantification of myofiber cross-sectional area (right). At least 10 measurements were performed per animal. The graph shows mean fiber area for n = 6 animals per group (7-month-old mice). (**B**) In vivo positron emission tomography and computed tomography analysis of skeletal muscle glucose uptake. Data are mean ± SEM of ^{18}F-FDG activity (n = 5, 4-month-old mice). SUV, standard uptake. (**C**) Forelimb grip strength analysis (n = 10-11, 7-month-old mice). (**D**) Relative mRNA levels of genes related to muscle proteolysis (*MuRF*-1 and *Atrogin-1*) and inflammation (*Stat1* and *IL-6*) (n = 7-8, 7-month-old mice). (**E**) Representative H&E stained sections of gWAT from *Tfam$^{fl/fl}$ Cd4^{Cre}* and *Tfam$^{fl/fl}$* mice (left, scale bar: 50 μm). The graph (right) shows mean estimated adipocyte surface area. Ten measurements were performed per animal (n = 5-6 animals, 7-month-old mice). (**F**) Percentage of adipose tissue determined by quantitative magnetic resonance imaging in *Tfam$^{fl/fl}$ Cd4^{Cre}* and *Tfam$^{fl/fl}$* mice (n = 6, 7-month-old mice). (**G**) Immunoblot (left) and densitometry analysis (right) of ATGL protein expression in gWAT isolated from *Tfam$^{fl/fl}$CD4^{Cre}* mice and control littermates (n = 6, 7-month-old mice). (**H**) Plasma non-esterified fatty acids (NEFA) (n = 7, 4-month-old mice). (**I**) Representative H&E-stained heart sections from 15-month-old *Tfam$^{fl/fl}$ Cd4^{Cre}* and *Tfam$^{fl/fl}$* mice. Scale bar: 2.5 mm (**J**) Echocardiography measurements of left ventricular (LV) mass in 3- and 15-month-old *Tfam$^{fl/fl}$* and *Tfam$^{fl/fl}$ Cd4^{Cre}* mice (n = 5-12). (**K**) Heart rate in 3-month-old *Tfam$^{fl/fl}$ Cd4^{Cre}* mice and control littermates (n = 9-10). (**L**) Cardiac output in 3- and 15-month-old *Tfam$^{fl/fl}$* and *Tfam$^{fl/fl}$ Cd4^{Cre}* mice (n = 5-11). (**M**) Lung weight normalized to tibia length in *Tfam$^{fl/fl}$* and *Tfam$^{fl/fl}$ Cd4^{Cre}* mice (n = 7-11, 7-month-old mice). (**N**) Mitral flow pattern on echocardiography in 3- and 15-month-old *Tfam$^{fl/fl}$* and *Tfam$^{fl/fl}$ Cd4^{Cre}* mice (n = 5-6). (**O**) Representative ultrasound images depicting maximal ascending aorta diameters in 15-month-old *Tfam$^{fl/fl}$* and *Tfam$^{fl/fl}$ Cd4^{Cre}* mice (left, scale bar: 1 mm) and quantification of maximal aortic diameter in 3- and 15-month-old *Tfam$^{fl/fl}$* and *Tfam$^{fl/fl}$ Cd4^{Cre}* mice (right) (n = 6-8). Maximal aortic diameter is presented in box-and-whisker plots showing maximal and minimal values and 75th and 25th percentiles. (**P**) RT-qPCR analysis of *Nos2*, *Acta2*, and *Myh11* mRNA expression levels in aortic samples from 7-month-old *Tfam$^{fl/fl}$* and *Tfam$^{fl/fl}$ Cd4^{Cre}* mice (n = 4). (**Q**) Systolic and diastolic blood pressure in 3-month-old *Tfam$^{fl/fl}$* and *Tfam$^{fl/fl}$ Cd4^{Cre}* mice (n = 9-10). (**R**) Representative CD3-stained brain (*fornix*) sections from 15-month-old *Tfam$^{fl/fl}$* and *Tfam$^{fl/fl}$ Cd4^{Cre}* mice (scale bar: 25 μm) and quantification of CD3 positive cell density (n = 6-10). (**S**) Rotarod test performance by *Tfam$^{fl/fl}$* and *Tfam$^{fl/fl}$ Cd4^{Cre}* mice, expressed as the mean time spent on the rotating rod in each of three trials (left) and all trials combined (right) (n = 7-10, 12-month-old mice). (**T**) Maximum clasping score per 30 s test (n = 8-9, 12-month-old mice). Dots in all panels represent individual sample data. Data are presented as means ± SEM. Box plots represent the median and the 25th and 75th percentiles. Statistical analysis was by unpaired Student's *t*-test [**A** to **C**, **D** (*MuRF-1*, *Atrogin*, *IL-6*), **F** to **L**, **N** and **O** (15mo), **P**, **Q** (Diastolic pressure) and **S**]; unpaired Welch's *t*-test [**D** (*Stat1*), **M** and **N** and **O** (3mo)]; or nonparametric Mann–Whitney *U* test [**Q** (Systolic pressure), **R** and **T**]. *p<0.05, **p<0.01, ***p<0.001, ****p<0.0001.

Fig. 3. ***Inflammaging induces senescence in distal tissues of Tfam$^{fl/fl}$ Cd4^{Cre} mice.***

(**A**) Heatmap of senescence gene expression changes comparing liver from *Tfam$^{fl/fl}$ Cd4^{Cre}* mice and control littermates. (**B**) Representative immunoblot (left) and quantification (right) of p21 and p53 protein expression in liver, heart, gWAT, and pancreas from *Tfam$^{fl/fl}$ Cd4^{Cre}* and *Tfam$^{fl/fl}$* mice. Loading controls were β-actin, H3, Hsp90 or α-tubulin (n = 4-7, 7-month-old mice) (**C**) Quantitative measurements of β-galactosidase activity in gWAT lysates by colorimetric assay (n = 6-9, 9-month-old mice). (**D**) Quantitative measurements of β-galactosidase activity in kidney lysates by colorimetric assay (n = 6-9, 12-month-old mice). (**E**) Immunoblot (left) and densitometry analysis (right) of p21 expression in immortalized mouse hepatocytes and 3T3-L1 cells cultured for 7 days in the presence of *Tfam$^{fl/fl}$* or *Tfam$^{fl/fl}$ Cd4^{Cre}* serum from 7-month-old mice. β-actin was used as a loading control (n = 4-6). Blots are representative of three (3T3-L1) or four (hepatocytes) experiments using pooled sera from three animals. (**F**) Representative immunoblot analysis of senescence markers in liver from control *Tfam$^{fl/fl}$* and *Tfam$^{fl/fl}$ Cd4^{Cre}* mice with or without treatment with anti-TNF-α (etanercept) (n = 6, 10 weeks of treatment starting from 4 months of age). (**G**) β-galactosidase activity measured by a colorimetric assay in kidney lysates (n = 6, 10 weeks of treatment). **(H)** Time course of forelimb strength during anti-TNF-α treatment. (**I**) Systolic blood pressure after 7 weeks of anti-TNF-α treatment (n = 6). (**J**) Maximal ascending aorta diameter in response to anti-TNF-α treatment (n = 6, 8 weeks of treatment). Maximal aortic diameter is presented in a box-and-whisker plots showing maximal and minimal values and 75th and 25th percentiles. (**K**) Y-Maze analysis in *Tfam$^{fl/fl}$ Cd4^{Cre}* mice treated with anti-TNF-α and corresponding controls (n = 6, 8 weeks of treatment). (**L-N**) Immunoblot (left) and densitometry analysis (right) of p21 or p53 expression in liver (**L**), gWAT (**M**), and tibialis muscle (**N**) from *Cd3e$^{-/-}$* mice 16 weeks after reconstitution with bone marrow from *Tfam$^{fl/fl}$ Cd4^{Cre}* or *Tfam$^{fl/fl}$* mice (n = 4-6 per group). Dots in all panels represent individual sample data. Data are presented as mean ± SEM. Statistical analysis was by one-way analysis of variance (ANOVA) with post hoc Tukey's correction [**G, I** and **K**]; Kruskal–Wallis test with post hoc Dunn's correction [**J**]; two-way ANOVA with post hoc Tukey's correction [**H**]; unpaired Student's *t*-test [**B**, **C**, **D**, **E**, **L** and **M**] or nonparametric Mann–Whitney *U* test [**N**]. *p<0.05, **p<0.01, ***p<0.001, ****p<0.0001.

Fig. 4. ***Nicotinamide riboside (NR) treatment rescues the multimorbidity syndrome.***

(**A, B**) NAD^+/NADH ratio in liver (A) and in isolated $CD4^+$ T cells (B) lysates from untreated *Tfam*$^{fl/fl}$, *Tfam*$^{fl/fl}$ *Cd4*^{Cre}, and NR-treated *Tfam*$^{fl/fl}$ *Cd4*^{Cre} mice (n = 5-9 per group, 10-week treatment starting from 4 months of age). (**C**) FACS analysis of intracellular T-bet (left), IFN-γ (center) and TNF-α (right) in splenic $CD4^+$ T cells (n = 8-17). (**D**) Effect of NR treatment on the evolution of forelimb strength (n = 5-11). (**E**) Heart rate (left), systolic blood pressure (center), and ascending aorta (AsAo) maximum diameter (right) obtained from ultrasound images after 8 weeks of NR treatment. Maximal aortic diameter is presented in a box-and-whisker plot showing the median and the 25th and 75th percentiles (n = 5-14). (**F**) RT-qPCR analysis of *Nos2*, *Acta2*, and *Myh11* mRNA expression in aorta from untreated *Tfam*$^{fl/fl}$, *Tfam*$^{fl/fl}$ *Cd4*^{Cre} and, NR-treated *Tfam*$^{fl/fl}$ *Cd4*^{Cre} mice (n = 4-6). (**G**) Blood hemoglobin levels (n = 4-7). (**H**) β-galactosidase activity measured by colorimetric assay in kidney lysates (n = 4-6). (**I**) Western blot (left) and densitometry analysis (right) of p21 and p53 expression in liver lysates from untreated *Tfam*$^{fl/fl}$, *Tfam*$^{fl/fl}$ *Cd4*^{Cre} and *Tfam*$^{fl/fl}$ *Cd4*^{Cre} mice treated with NR for 10 weeks (n = 3-4). β-actin was used as a loading control. (**J**) Circulating TNF-α determined by Multiplex analysis in serum from untreated *Tfam*$^{fl/fl}$, *Tfam*$^{fl/fl}$ *Cd4*^{Cre}, and NR-treated *Tfam*$^{fl/fl}$ *Cd4*^{Cre} mice (n = 5-8). (**K**) Activity (left) and energy expenditure (right) monitored over a 24-hour cycle in metabolic cages (n = 4-5). (**L**) Principal component (PC) analysis of transcriptomics in liver samples from untreated *Tfam*$^{fl/fl}$, *Tfam*$^{fl/fl}$ *Cd4*^{Cre} and *Tfam*$^{fl/fl}$ *Cd4*^{Cre} mice treated with NR for 10 weeks (n = 3-4). (**M**) IPA heatmap showing transcriptionally altered cellular pathways. Dots in all panels represent individual sample data. Data are presented as mean ± SEM. Statistical analysis was by one-way analysis of variance (ANOVA) with post hoc Tuley's correction [**A** to **C**, **E** (Maximal aortic diameter), **G**, **H**, **I** (p21), **J and K** (Energy expenditure)]; Kruskal–Wallis *H* test with post hoc Dunn's correction [**E** (Heart rate and Systolic blood pressure), **F**, **I** (p53) and **K** (Activity)]; or two-way ANOVA with correction post hoc Tukey's correction [**D**]. *p<0.05, **p<0.01, ***p<0.001, ****p<0.0001.

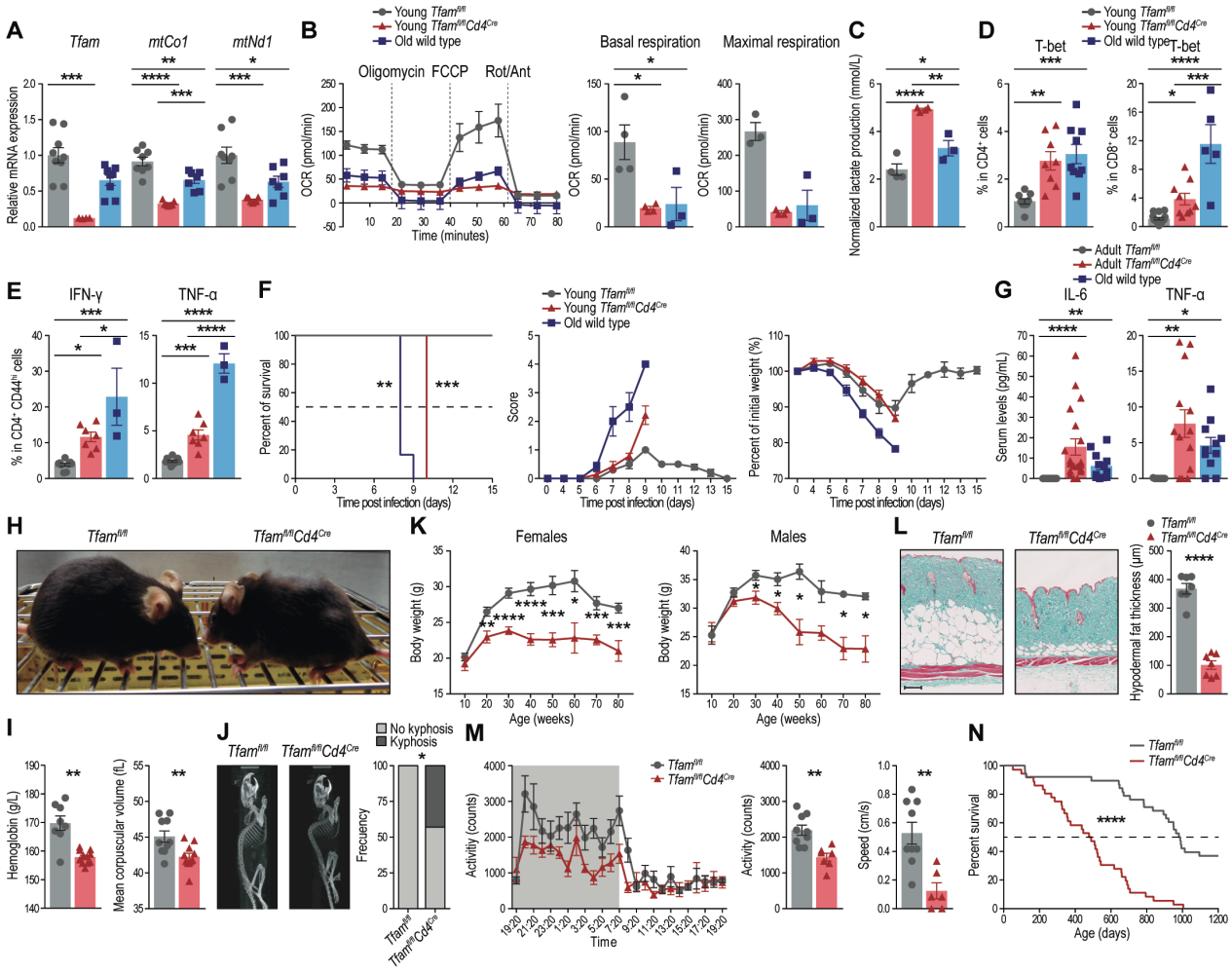
A
Tfam
mtCo1
mtNd1
Relative mRNA expression
B
Young Tfam^fl/fl
Young Tfam^fl/fl Cd4^Cre
Old wild type
Oligomycin
FCCP
Rot/Ant
OCR (pmol/min)
Time (minutes)
Basal respiration
Maximal respiration
C
Normalized lactate production (mmol/L)
D
T-bet
% in CD4+ cells
% in CD8+ cells
E
IFN-γ
TNF-α
% in CD4+ CD44hi cells
F
Percent of survival
Time post infection (days)
Score
Percent of initial weight (%)
G
Adult Tfam^fl/fl
Adult Tfam^fl/fl Cd4^Cre
IL-6
TNF-α
Serum levels (pg/mL)
H
Tfam^fl/fl
Tfam^fl/fl Cd4^Cre
K
Females
Males
Body weight (g)
Age (weeks)
L
Hypodermal fat thickness (μm)
I
Hemoglobin (g/L)
Mean corpuscular volume (fL)
J
No kyphosis
Kyphosis
Frecuency
M
Activity (counts)
Time
Speed (cm/s)
N
Percent survival
Age (days)

Fig. 1.

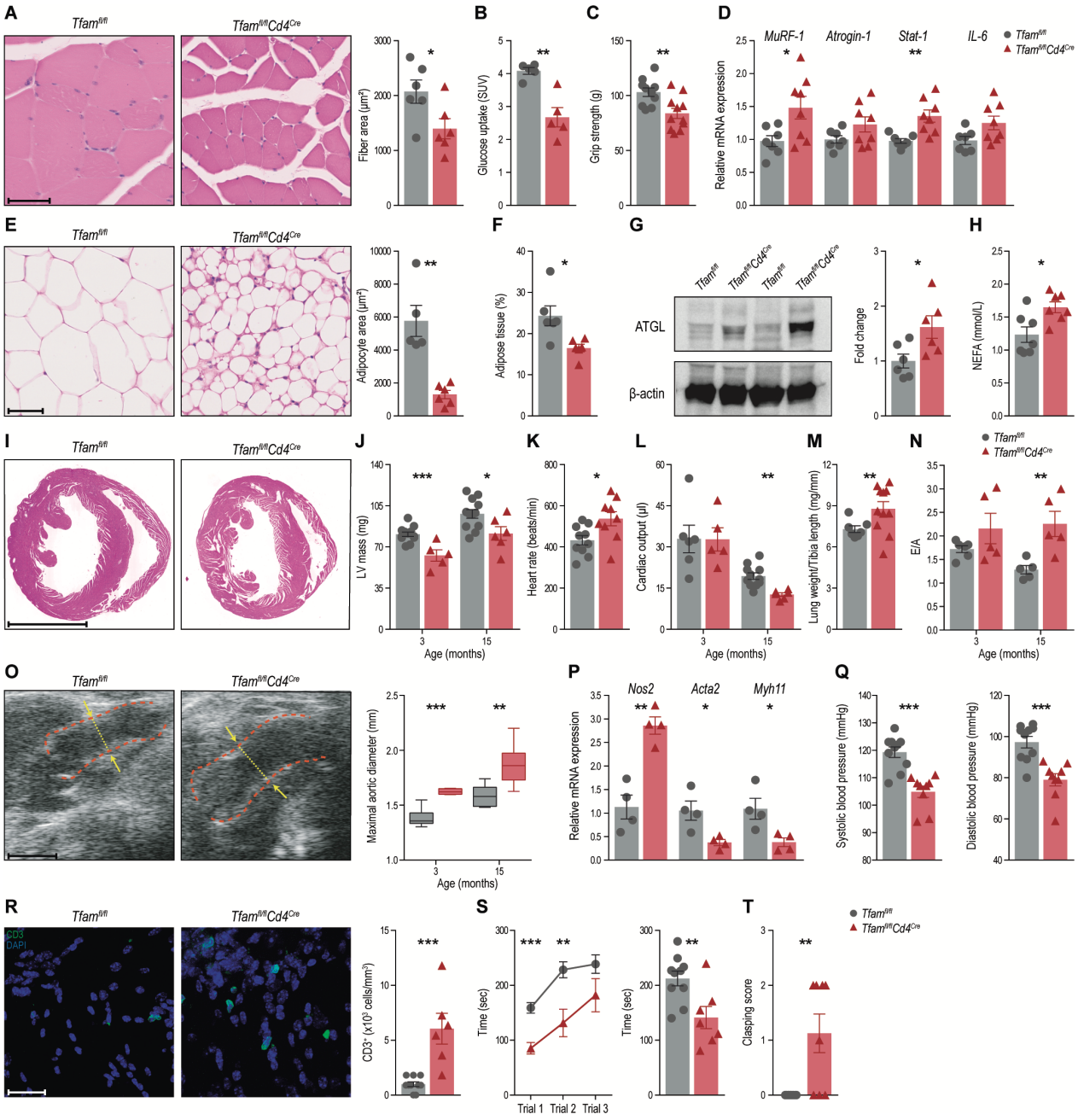
A
Tfam^fl/fl
Tfam^fl/flCd4^Cre
Fiber area (μm²)
B
Glucose uptake (SUV)
C
Grip strength (g)
D
MuRF-1
Atrogin-1
Stat-1
IL-6
Relative mRNA expression
E
Adipocyte area (μm²)
F
Adipose tissue (%)
G
ATGL
β-actin
Fold change
H
NEFA (mmol/L)
I
J
LV mass (mg)
K
Heart rate (beats/min)
L
Cardiac output (μl)
M
Lung weight/Tibia length (mg/mm)
N
E/A
Age (months)
O
Maximal aortic diameter (mm)
P
Nos2
Acta2
Myh11
Q
Systolic blood pressure (mmHg)
Diastolic blood pressure (mmHg)
R
CD3
DAPI
CD3⁺ (x10³ cells/mm³)
S
Time (sec)
Trial 1
Trial 2
Trial 3
T
Clasping score

Fig. 2

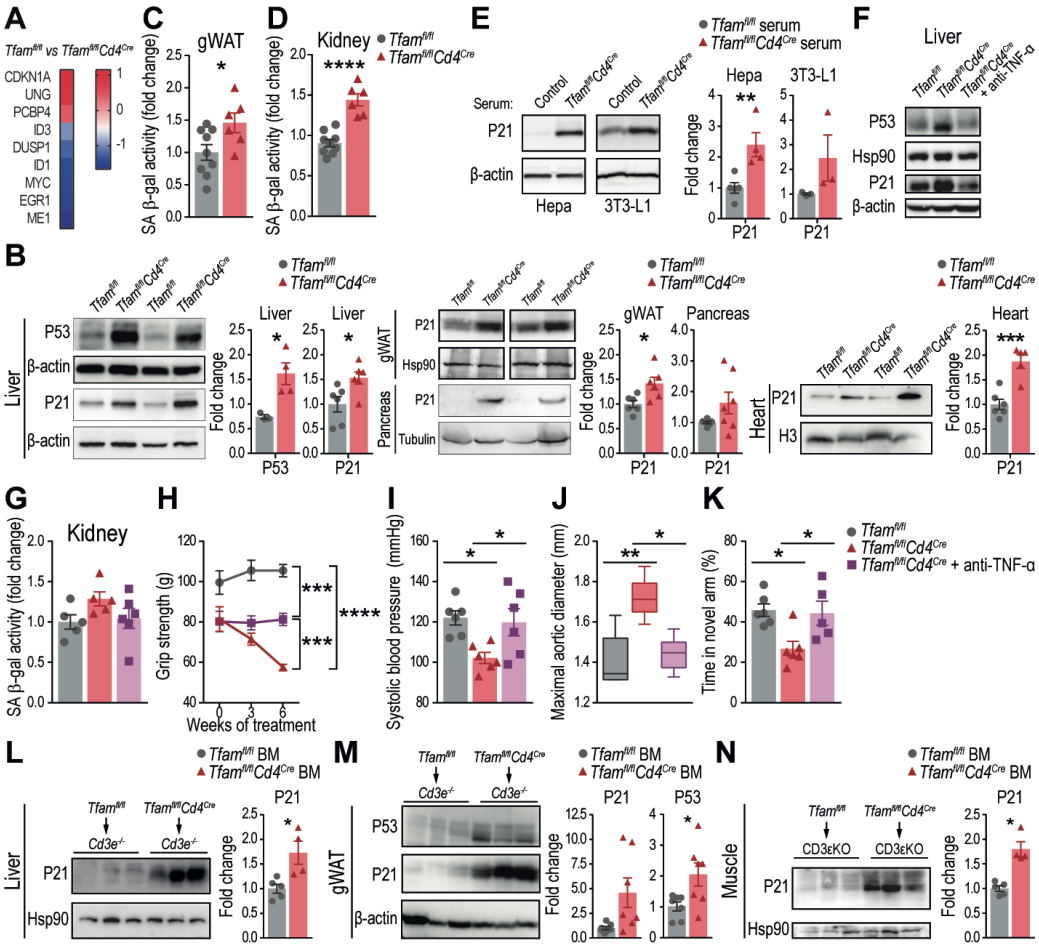
A
Tfam fl/fl vs Tfam fl/fl Cd4Cre
CDKN1A
UNG
PCBP4
ID3
DUSP1
ID1
MYC
EGR1
ME1
C
gWAT
SA β-gal activity (fold change)
D
Kidney
Tfam fl/fl
Tfam fl/fl Cd4Cre
E
Serum:
Control
Tfam fl/fl Cd4Cre
P21
β-actin
Hepa
3T3-L1
Tfam fl/fl serum
Tfam fl/fl Cd4Cre serum
Fold change
F
Liver
Tfam fl/fl
Tfam fl/fl Cd4Cre
Tfam fl/fl Cd4Cre + anti-TNF-α
P53
Hsp90
B
Liver
gWAT
Pancreas
Heart
Tubulin
H3
G
H
Grip strength (g)
Weeks of treatment
I
Systolic blood pressure (mmHg)
J
Maximal aortic diameter (mm)
K
Time in novel arm (%)
Tfam fl/fl Cd4Cre + anti-TNF-α
L
BM
Cd3e-/-
M
N
Muscle
CD3εKO

Fig. 3

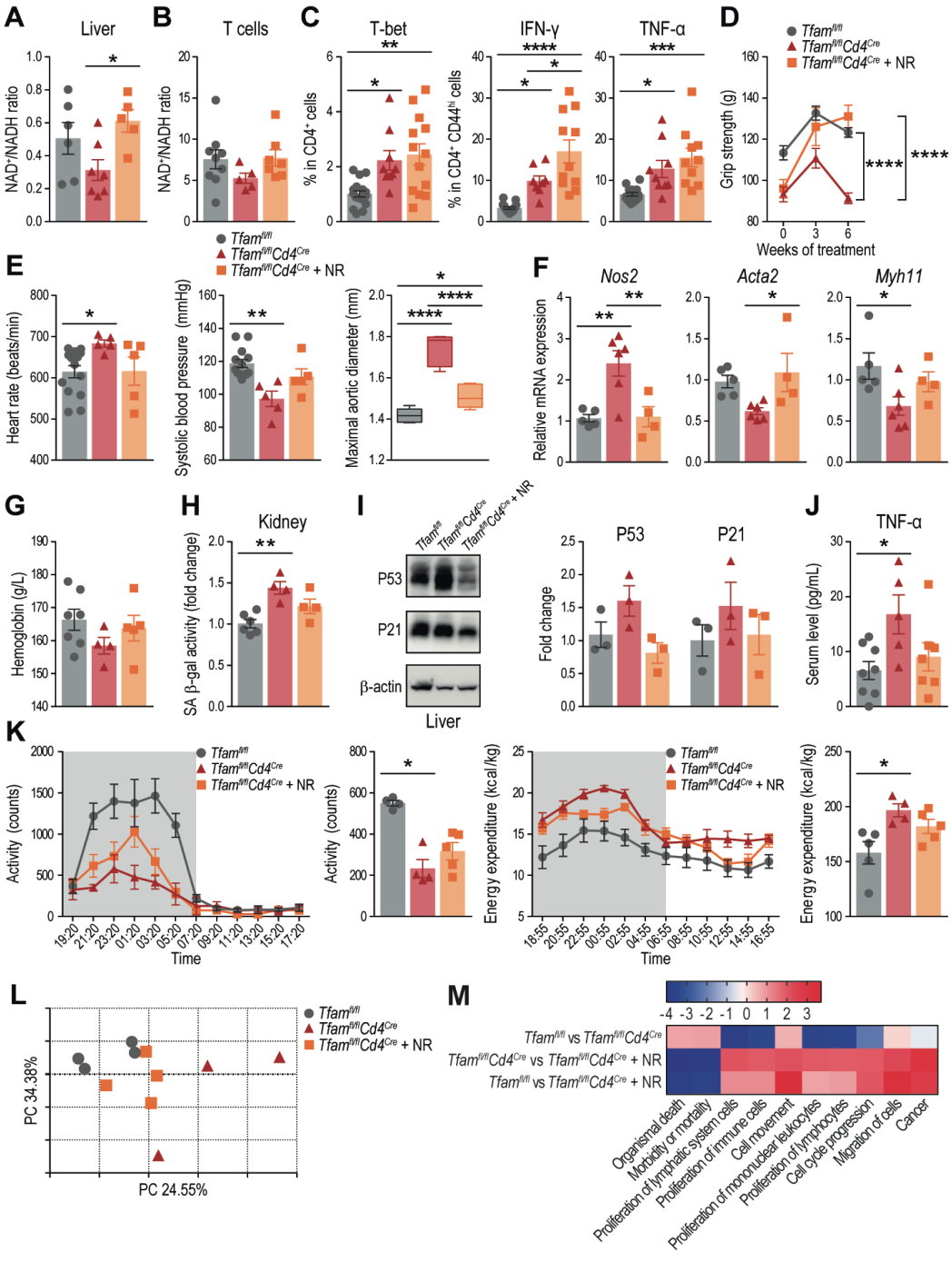
A
Liver
NAD+/NADH ratio
B
T cells
NAD+/NADH ratio
C
T-bet
% in CD4+ cells
IFN-γ
% in CD4+ CD44hi cells
TNF-α
D
Tfam fl/fl
Tfam fl/fl Cd4Cre
Tfam fl/fl Cd4Cre + NR
Grip strength (g)
Weeks of treatment
E
Heart rate (beats/min)
Systolic blood pressure (mmHg)
Maximal aortic diameter (mm)
F
Nos2
Acta2
Myh11
Relative mRNA expression
G
Hemoglobin (g/L)
H
Kidney
SA β-gal activity (fold change)
I
P53
P21
β-actin
Liver
Fold change
J
TNF-α
Serum level (pg/mL)
K
Activity (counts)
Time
Energy expenditure (kcal/kg)
L
PC 34.38%
PC 24.55%
M
Tfam fl/fl vs Tfam fl/fl Cd4Cre
Tfam fl/fl Cd4Cre vs Tfam fl/fl Cd4Cre + NR
Tfam fl/fl vs Tfam fl/fl Cd4Cre + NR
Organismal death
Morbidity or mortality
Proliferation of lymphatic system cells
Proliferation of immune cells
Cell movement
Proliferation of mononuclear leukocytes
Proliferation of lymphocytes
Cell cycle progression
Migration of cells
Cancer

Fig. 4

Supplementary Materials for

Immunometabolic T cell failure induces multimorbidity and aging

Gabriela Desdín-Micó[1,2], Gonzalo Soto-Heredero[1,2]†, Juan Francisco Aranda[1,2]†, Jorge Oller[1,2]†, Elisa Carrasco[1,2], Enrique Gabandé-Rodríguez[1,2], Eva Maria Blanco[1,2], Arantzazu Alfranca [3], Lorena Cusso[4,5], Manuel Desco[4,5], Borja Ibañez[5,6,7], Arancha R. Gortazar[8], Pablo Fernández-Marcos[9], Maria N. Navarro[2,3], Bruno Hernaez[2], Antonio Alcamí[2], Francesc Baixauli[10] and María Mittelbrunn[1,2]*

Correspondence to: mmittelbrunn@cbm.csic.es

This PDF file includes:

Materials and Methods

Figs. S1 to S6

Other Supplementary Material for this manuscript includes the following:

Table S1 (Microsoft Excel format). IPA analysis of upstream regulators involved in NR protection.

Supplementary references:28-30

Materials and Methods

Animal procedures

Tfam$^{fl/fl}$ *Cd4*^{Cre} (*Cd4*^{Cre} mice JAX stock #017336, (*28, 29*)) mice were generated as previously described (*13*). *Tfam*$^{fl/fl}$ littermates not expressing Cre were used as control mice along the study. All animal procedures complied with the 2010/63/UE European guideline and were approved by the Animal Experimentation Ethics Committees of the Centro de Biología Molecular "Severo Ochoa" (CBMSO), Universidad Autónoma de Madrid (UAM) or the Centro Nacional de Investigaciones Cardiovasculares Carlos III (CNIC). *Lck*^{Cre} mice (JAX stock #003802,(*30*)) were kindly provided by Prof. B. Alarcón and were bred with *Tfam*$^{fl/fl}$ to generate *Tfam*$^{fl/fl}$ (control mice) and *Tfam*$^{fl/fl}$ *Lck*^{Cre} animals. For some experiements, mice were grouped into three different age categories; young (less than 4 months of age); adults (4 to 18 months of age) and old (over 18 months of age).

For infection experiments, groups of six mice per condition were anesthetized with isofluorane and infected by subcutaneous inoculation into the footpad with 10 µL of PBS with 0.1% bovine serum albumin and containing 10^3 PFUs of sucrose semipurified Ectromelia virus (ECTV) Naval strain, grown in BSC1 cells. Mice were housed in ventilated racks under biological safety level 3 containment facilities, weighted and monitored daily for survival, signs of mousepox disease and footpad swelling of the inoculated hind leg. Mice were sacrificed after reaching established humane endpoints.

For cardiovascular analysis, arterial blood pressure was measured in mouse tails with the automated BP-2000 Blood Pressure Analysis System (Visitech Systems, Apex, NC, USA). For ultrasound imaging, cardiac and aortic parameters were monitored in isofluorane-anesthetized mice (1%) by high-frequency ultrasound using a Vevo 2100 echocardiography device (VisualSonics, Toronto, Canada) with 30-µm resolution limit. All recordings were made by a technician blinded to animal genotype and treatment. Limb grip strength was measured as tension force using a digital force transducer (Grip Strength Meter, Bioseb). Three measurements per trial were performed for each animal, with a few seconds resting period between measurements. Food intake and other metabolic parameters were measured using PhenoMaster TSE-Systems (Germany). Mice were singly housed and acclimatized for 3 days before data monitoring. All parameters were measured continuously and simultaneously over 3 days. The treatments of *Tfam*$^{fl/fl}$ *Cd4*^{Cre} mice with NR (Novalix) or Etanercept (Benepali®) started at the age of 4 months. NR was administered intraperitoneally at

1000 mg/kg in 0.9% NaCl every other day for 10 weeks. For anti-TNF-α treatment, mice were injected intraperitoneally every other day with 100 µg of etanercept (Benepali®) in 0.9% NaCl for 10 weeks, using 0.9% NaCl as vehicle control. Aged C57BL/6 were purchased from Envigo. Eight-month-old and 19-month-old wt mice were treated with saline (control) or NR. Four groups were treated for over 10 weeks. Blood was then collected to isolate serum.

For hematological analysis, blood was collected in potassium EDTA microtrainer tubes via a superficial temporal vein. Complete blood count was performed in Abacus Junior hematology analyzer. NEFA quantification was performed in Dimension RxL Max analyzer. For bone marrow reconstitution experiments, 8-to-12-week-old T cell-deficient mice (*Cd3e*$^{-/-}$, JAX stock #004177, kindly provided by Prof. B. Alarcón) were sublethally irradiated with 9 Gy (2 x 4.5 Gy). Subsequently, 5 × 10^6 bone marrow cells from *Tfam*$^{fl/fl}$ or *Tfam*$^{fl/fl}$ *Cd4*^{Cre} mice were injected into each recipient mouse via retro orbital sinus. Glucose uptake was studied by positron emission computed tomography (PET–CT) with a small-animal PET–CT device (Mediso Medical Imaging Systems, Budapest). Animals were weighed, and 0.2 ml of 8-10 MBq ^{18}F-FDG was injected intravenously through a lateral tail vein. Blood glucose levels were measured before the administration of ^{18}F-FDG. Animals were anesthetized with a mixture of 1.5-2% isofluorane in oxygen at 3 liter/min and kept at 38ºC throughout the procedure. CT scanning was performed first, followed by metabolic PET static acquisition for 15 min. Images were analyzed with AMIDE software. Angles below 15% of the average controls were classified as kyphosis. For each animal study, the PET image was aligned with the CT image. Regions of interest (ROI) were drawn for major organs (heart and gastrocnemius muscle). Standardized uptake value (SUV) was calculated for each animal. Magnetic resonance imaging (MRI) of body fat content was performed by using a 7-T Agilent/Varian scanner (Agilent, Santa Clara, CA, USA) equipped with a DD2 console. For image acquisition, mice were deeply sedated using isoflurane at 2% and 1.8 liter/min oxygen flow. Ophthalmic gel was placed in the eyes of mice to prevent retinal drying. Images were obtained using a *SEMS* sequence without fat saturation with the following parameters: TR/TE = 533-884 /10.44 ms (TR varies between with and without fat saturation); acquisition matrix 128 × 128; flip angle 90^o; 1 average; 35 slices; slice thickness: 1 mm; and gap: 1 mm. Body and abdominal fat content were analyzed using Image J (*http://imagej.nih.gov*). Fat was segmented from each slice to obtain its corresponding area, which was multiplied by the slice distance to obtain the fat volume. Fat mass was estimated by the product between fat volume and fat density (0.9 g/cm^3).

Autoantibodies in mouse serum were measured using QuantaLite®ANA and QuantaLIte®ENA6 ELISA kits (INOVA) following manufacturer's instructions, except for secondary antibody, which was substituted with anti-mouse IgG-HRP (Thermo Scientific, 100 ng/mL). Motor coordination was assessed by performing the rotarod test in an accelerating rotarod apparatus (Ugo Basile, Varese, Italy). Mice were trained for 2 days at a constant speed: on the first day, four times at 4 r.p.m. for 1 min and on the second day four times at 8 r.p.m. for 1 min. On the third day, the Rotarod was set to progressively accelerate from 4 to 40 r.p.m for 5 min. Mice were tested three times. During the accelerating trials, the latency to fall from the rod was measured. For hindlimb clasping score analysis in the tail suspension test, mice were suspended by their tails for 30 s and video-recorded. Animals were assessed for maximum clasping score in the tail suspension test (maintained for at least 4 consecutive seconds). An animal would receive a score of 0 points if both hindlimbs were splayed outward away from the body, with splayed toes. Hindlimb clasping was scored as; 1, one hindlimb retracted towards the body, 2, two hindlimbs retracted towards the body, 3, both hindlimbs retracted towards the body and contacting both forelimbs. Spatial learning was analyzed in the Y-Maze test that measures the willingness of mice to explore a new environment. Mice were allowed to explore in the training trial for 7 min, with access to two of the three arms (the initial arm and one other arm), maintaining the third or novel arm closed. After 1 hour, the mice were placed in the same starting arm with free access to all three arms for 5 min. The time spent in the novel arm was counted and expressed as a percentage of the total exploration time.

ELISA and Luminex detection of proinflammatory cytokines

Serum cytokines were detected with magnetic bead technology (Invitrogen, Th1/Th2/Th9/Th17/Th22/Treg Cytokine 17-Plex Mouse ProcartaPlex™ PanelLuminex) and MILLIPLEX MAP Mouse High Sensitivity T Cell Panel for IL-6 and TNF-α (MHSTCMAG-70K, Merck Chemicals). IL-6 was detected with an ELISA kit (Diaclone).

Cell culture

All cell cultures were maintained at 37ºC and 5% CO_2. Mouse immortalized hepatocytes (Hepa) were kindly provided by Dr. Sabio (Centro Nacional de Investigaciones Cardiovasculares, Madrid)

and were cultured in DMEM supplemented with 10% fetal bovine serum (FBS) and an antibiotic solution containing penicillin–streptomycin. The preadipocyte cell line 3T3-L1 was cultured in DMEM, 10% FBS. Senescence was induced in vitro by replacing FBS with serum from *Tfam*$^{fl/fl}$ *Cd4*^{Cre} mice, using serum from *Tfam*$^{fl/fl}$ counterparts as a control. Sera from individual animals were pooled and added at 1-2% to hepatocytes or 3T3-L1 preadipocytes which were maintained under these conditions for 7 days, with a medium change on day 4.

RNA extraction and Real-Time PCR

For the assessment of mtDNA, mtRNA (*mtNd1* and *mtCo1*) and *Tfam* RNA levels in circulating CD4$^+$ T cells, blood samples were collected from 2-month-old *Tfam*$^{fl/fl}$, *Tfam*$^{fl/fl}$ *Cd4*^{Cre} or 22-month-old wt mice and CD4$^+$ T cells were isolated by cell sorting in a FACSAria Fusion (Becton Dickinson). CD4$^+$ T cells were gated on viable CD3$^+$. RNA extraction was performed with FisherBioReagents™ SurePrep™ RNA/DNA/Protein Purification Kit (Fisher Scientific, 10562474).

Total RNA was extracted from frozen tissue with Trizol reagent (Invitrogen™) and ceramic beads using a MagNa lyser instrument (Roche). RNA was purified using the RNeasy Mini Kit (QIAGEN) and was retrotranscribed to cDNA with the Maxima™ First Strand cDNA Synthesis Kit and dsDNase (Thermo Fisher Scientific). Real-time quantitative RT-PCR (qPCR) reactions were performed with PowerUp™ SYBR™ Green Master Mix in 384-well plates in an ABI PRISM 7900 Real-Time PCR thermocycler (Applied Biosystems). The following primers were used for qPCR: *Acta2* (5′-ATCGTCCACCGCAAATGC-3′, 5′-AAGGAACTGGAGGCGCTG-3′), *Mmyh11*(5′-TCAACGCCAACCGCAGGAAGCTG-3′, 5′-TGCTAAGCAGTCTGCTGGGCT-3′), *Nos2* (5′-CAGCTGGGCTGTACAAACCTT-3′, 5′-CATTGGAAGTGAAGCGTTTCG-3′), *Foxo3a* (5′-CAGGCTCCTCACTGTATTCAGCTA-3′, 5′-CATTGAACATGTCCAG GTCCAA-3′), *Nppa* (5′-AGCCGAGACAGCAAACATCAG-3′, 5′-CAAAAGGCCAGGAAGAGGAAG-3′), *Il-6* (5′-GTCTATACCACTTCACAAGTC-3′, 5′-TGCATCATCGTTGTTCATAC-3′), *Atrogin-1* (5′-CTGAAAGTTCTTGAAGACCAG-3′, 5′-GTGTGCATAAGGATGTGTAG-3′), *Murf-1* (5′-GGGTAAAGAAGAACACCAATG-3′, 5′-GAAGACACACTTCCCTATTG-3′), *Stat1* (5′-GCTTGACAATAAGAGAAAGGAG-3′, 5′-CTCGTCATTAATCAGAGTGTTC-3′), *mtCO1* (5′-CTCGCCTAATTTATTCCACTTCA-3′, 5′-

GGGGCTAGGGGTAGGGTTAT-3′), *mtND1* (5′-GGGATAACAGCGCAATCCTA-3′, 5′-ATCGTTGAACAAACGAACCA-3′) , *Tfam* (5′-CAGGAGGCAAAGGATGATTC-3′, 5′-CCAAGACTTCATTTCATTGTCG-3′). At least two different reference targets were used to normalized among these: *B2m* (5′-TACATACGCCTGCAGAGTTAAGCA-3′, TGATCACATGTCTCGATCCCAG-3′), *Ppia* (ACGCCACTGTCGCTTTTC-3′, 5′-GCAAACAGCTCGAAGGAGAC-3′), *Ywhaz* (5′-TTACTTGGCCGAGGTTGCT-3′, 5′-TGCTGTGACTGGTCCACAAT-3′), *Actb* (5′-CTAAGGCCAACCGTGAAAAG-3′, 5′-ACCAGAGGCATACAGGGACA-3′). Relative expression was calculated as $RQ = 2^{-\Delta\Delta Ct}$.

NAD$^+$ and NADH measurements

NAD$^+$ and NADH levels and the NAD$^+$/NADH ratio were measured in frozen tissue samples using the NAD$^+$/NADH kit (Biovision). For T cells, CD4$^+$ T cells were isolated from spleen and lymph nodes with EasySep™ Mouse CD4$^+$ T Cell Isolation Kit (Stemcell, 19852).

Flow cytometry and immunoblot analysis

Red blood cells were removed by incubation with a lysis buffer. For flow cytometry analyses, cells were sequentially incubated with Purified rat anti-mouse CD16/CD32 (BD Biosciences, 553142) and conjugated primary antibodies. The following antibodies were used: PerCP-Cy5.5-conjugated rat anti-human/mouse CD44 (0.1 µg/mL, Tonbo Biosciences, IM7, 65-0441), APC-conjugated mouse anti-mouse T-bet (0.2 µg/mL, Biolegend, 4B10, 644814), APC-conjugated rat anti-mouse TNF-α (0.2 µg/mL, Biolegend, MP6-XT22, 506308), FITC-conjugated rat anti-mouse IFN-γ (0.5 µg/mL, Tonbo Biosciences, XMG1.2, 35-7311), VioletFluor™ 450-conjugated rat anti-mouse CD4 (0.1 µg/mL, Tonbo Biosciences, GK1.5, 75-0041), PE-conjugated rat anti-mouse CD8a (0.1 µg/mL, Tonbo Biosciences, 53-6.7, 50-0081), and APC-Cy7-conjugated rat anti-mouse CD8 (0.1 µg/mL, Tonbo Biosciences, 53-6.7, 25-0081). Samples were assessed with a FACSCanto II cell analyzer (Becton Dickinson) using DiVA 8 acquisition software and FlowJo V10 data analysis software. For immunoblot analysis, cells or frozen tissue samples were lysed at 4ºC in RIPA buffer containing protease and phosphatase inhibitors cocktail (Sigma). Proteins were separated by SDS–PAGE and transferred onto 0.45 µm pore size Immobilon PVDF membrane (Millipore). PVDF membranes were blocked with TBS-T (50 mM Tris, 150 mM NaCl, and 0.1% Tween-20)

containing 5% (w/v) BSA or milk. Membranes were incubated with primary antibodies diluted 1/500 to 1/10.000 followed by TBS-T washes and incubation with HRP-conjugated secondary antibodies (GE Healthcare). The signal was visualized by enhanced chemiluminescence with Luminata Forte Western HRP Substrate (Millipore) and the ImageQuant LAS 4000 imaging system. The following antibodies were used: rabbit anti-mouse ATGL antibody (0.19 ng/mL, Cell Signaling, #2138), mouse anti-mouse α-tubulin antibody (0.355 ng/mL , Cell Signaling, #3873), mouse anti-mouse β-actin antibody (HRP) (0.32 µg/mL, Abcam, ab49900), donkey anti-rabbit IgG, HRP- conjugated antibody (0.08 µg/mL, Amersham Bioscience, NA934), sheep anti-mouse IgG, HRP-conjugated antibody (0.08 µg/mL, Amersham Bioscience, NA931), mouse anti-mouse p21 Waf1/Cip1 antibody (0.5 µg/mL, BD Biosciences, 556431), mouse anti-mouse MuRF1 antibody (0.4 µg/mL, Santa Cruz, sc-514767), mouse anti-mouse p53 antibody (0.2 µg/mL, Santa Cruz, sc-98), mouse anti-mouse Hsp90 antibody (0.25 µg/mL, BD Biosciences, 610418), rabbit anti-mouse Histone H3 antibody (1 µg/mL, Abcam, ab1791) and rabbit anti-mouse Fbx32 (Atrogin) antibody (0.5 µg/mL, Abcam, ab198958).

Seahorse and lactate measurements

$CD4^+$ T cells were purified from the spleen and lymph nodes of 2-month-old *Tfam*$^{fl/fl}$, *Tfam*$^{fl/fl}$ *Cd4*^{Cre} or 22-month-old wt mice. $CD4^+$ T cells were activated in RPMI-1640-complete medium with plate bound anti-CD3 (Tonbo Biosciences, 17A2, 70-0032, 5µg/mL), and anti-CD28 antibodies (Tonbo Biosciences, 37.51, 70-0281, 2µg/mL) for 48 hours. OCR and ECAR in $CD4^+$ T cells were measured in an XF96 extracellular flux analyzer (Seahorse Bioscience). Extracellular lactate determination was performed with Accutrend ® Plus system (Roche). We analyzed 20 µL of conditioned medium after 48 hours of activation. Lactate mesuarements were normalized to cell numbers.

Library preparation and Illumina sequencing

Libraries were prepared according to the instructions of the Kit "NEBNext Ultra Directional RNA Library Prep kit for Illumina" (New England Biolabs), following the protocol "Poly(A) mRNA

Magnetic Isolation Module". The input yield of total RNA to start the protocol was >300 ng quantified by an Agilent 2100 Bioanalyzer using a RNA 6000 nano LabChip kit. The fragmentation time used was 15 minutes. We performed the library amplification included in the citated protocol using a PCR of 13 cycles. The obtained libraries were validated and quantified by an Agilent 2100 Bioanalyzer using a DNA7500 LabChip kit and an equimolecular pool of libraries was titrated by quantitative PCR using the "Kapa-SYBR FAST qPCR kit forLightCycler480" (Kapa BioSystems) and a reference standard for quantification. The pool of libraries was denatured prior to be seeded on a flowcell at a density of 2.2 pM, where clusters were formed and sequenced using a "NextSeq™ 500 High Output Kit", in a 1 × 75 single read sequencing run on a NextSeq500 sequencer. Approximately 1×10^7 pass-filter reads were obtained for each sample, which was used for further bioinformatics analysis. Fastq files were aligned against Mm version1o genome using STAR aligner (base Space Sequence Hub, Illumina) and gene expression profiles were determined using CuffDiff2. Ingenuity Pathway Analysis (IPA) was used to identify cellular biological functions, genes clusters and upstream regulators.

Histological procedures

Hydrated paraffin sections or OCT cryosections were fixed with 10% neutral buffered formalin and stained as detailed in the figure legends. Digitized images were obtained with NDP.view 2 software. For brain immunofluorescence, cryostat sections were incubated overnight at 4°C with rabbit anti-CD3 (1 µg/mL, Abcam, ab5690) and then with an Alexa 488- conjugated donkey anti-rabbit secondary antibody (0.2 µg/mL, Thermo Fisher, A-21206). Finally, the sections were incubated for 10 min with DAPI (Calbiochem), washed and mounted with Prolong Gold Antifade (Invitrogen). Images were obtained in a LSM800 microscope (Carl Zeiss) equipped with 2 highly sensitive GaAsp detectors using a 63x oil-immersion objective. To quantify the density of $CD3^+$ cells, we applied unbiased stereology by using the optical disector method. Briefly, for each animal, the number of $CD3^+$ cells was quantified in z-stack images of 3 randomly selected areas in one of every five sections and the density of cells per volume of the whole fornix was stimated by using the Fiji software.

Senescence-associated β-galactosidase staining and quantitative assay

For the β-galactosidase quantitative assay, tissues were lysed with T-PER Tissue Protein Extraction Reagent (Thermo Scientific, 78510). Lysates were centrifuged at 10,000 × *g* for 5 min and the supernatant was collected. Fifty microliters of protein lysates were mixed with 50 µL of Pierce β-galactosidase Assay Reagent (Thermo Scientific, 75705) for the assay. The reaction was incubated for 30 min and the absorbance was measured at 405 nm. Values were normalized to total protein levels. Senescence-associated-β-gal (SA-β-Gal) activity imaging was performed using a β-gal staining kit (Cell Signaling Technology, #9860) at pH 6, according to the manufacturer's instructions.

Statistical analyses

Sample size is detailed in the corresponding figure legends. All experiments included at least three biological replicates. Statistical analyses were performed with GraphPad Prism 7. Before data analysis, outliers were checked, identified and excluded by using the ROUT method (Q value = 5%) to identified outilers provided with GraphPad Prism 7. Bar plots show mean ± standard error of the mean (SEM). Aortic diameter is presented in box-and-whisker plots showing maximal and minimal values and 75th and 25th percentiles. Data were analyzed for normality using the Shapiro–Wilk normality test. Statistical differences of two groups were assessed using unpaired Student's *t* test, *t*-test with Welch's correction for variance or Mann–Whitney *U* test where appropriate. Statistical differences of three groups were analyzed using analysis of variance (one-way ANOVA) with the Tukey post hoc test (Experiments with ≥ 3 groups) or Kruskal–Wallis *H* test where appropriate. To observe time-wise differences, two-way repeated-measures (two-way ANOVA) with Sidak post hoc test was used. Survival curve differences were analyzed with the log-rank (Mantel–Cox) test. Statistical significance was assigned at *p<0.05, **p<0.01, ***p<0.001, and ****p<0.0001.

Supplementary Figures

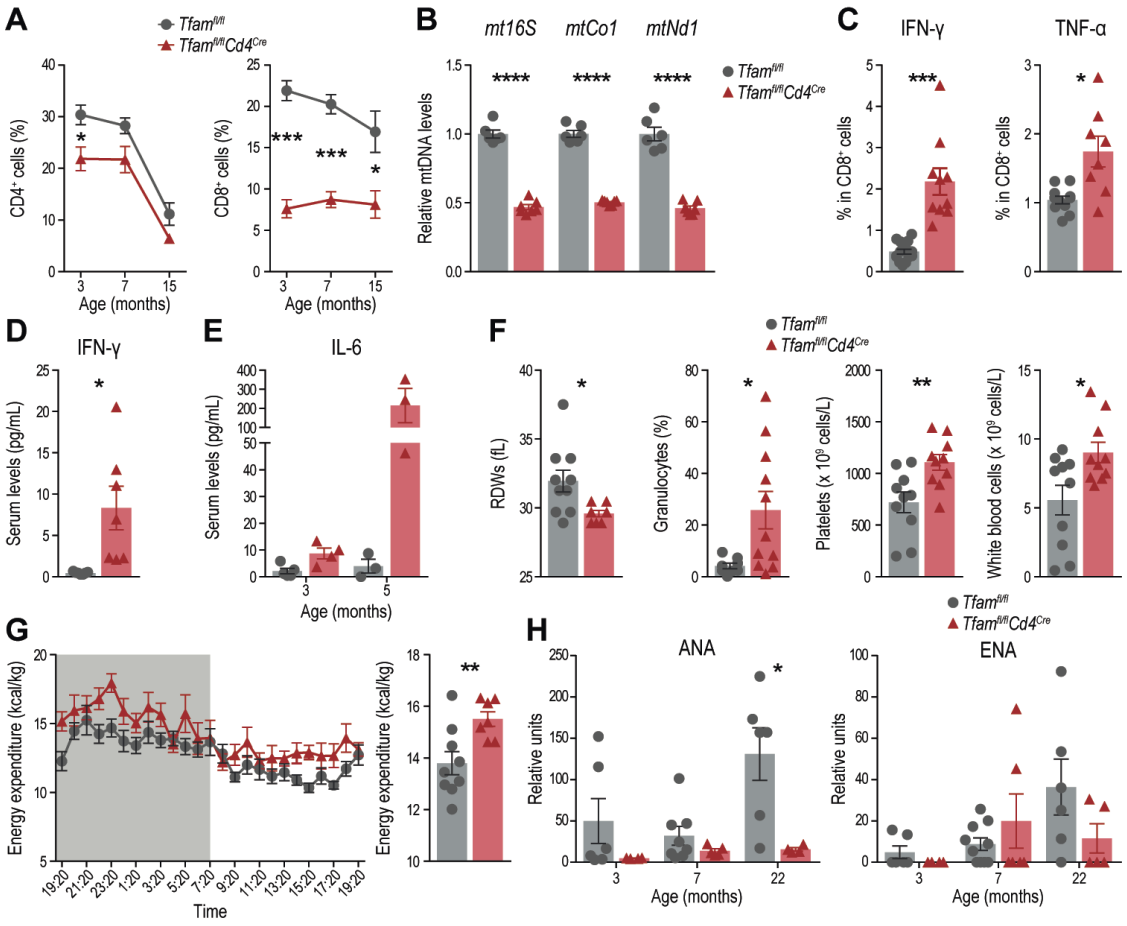

Fig. S1

Fig. S1. Premature aging phenotype of *Tfam*$^{fl/fl}$ *Cd4*^{Cre} mice.

(**A**) Percentages of CD4^{+} (left) and CD8^{+} (right) circulating T cells were longitudinally measured in whole blood from 3- to 15-month-old *Tfam*$^{fl/fl}$ and *Tfam*$^{fl/fl}$ *Cd4*^{Cre} (n = 3-7 per group). (**B**) mtDNA levels (*mt16S*, *mtCo1*, *mtNd1*) relative to nuclear DNA (*B2m* and *Actb*) in *Tfam*$^{fl/fl}$ and *Tfam*$^{fl/fl}$ *Cd4*^{Cre} CD4^{+} T cells (n = 6-7). (**C**) Percentages of IFN-γ (left) and TNF-α (right) positive cells in total CD8^{+} T cells (n = 8-15). (**D**) Serum levels of IFN-γ in 7-month-old *Tfam*$^{fl/fl}$ and *Tfam*$^{fl/fl}$ *Cd4*^{Cre} mice (n = 7). (**E**) ELISA analysis of circulating IL-6 levels in mice aged 3- and 5-month-old mice (n = 3-5). (**F**) Hematological red cell distribution width (RDWs), granulocyte percentage, platelets, and white blood cell numbers in *Tfam*$^{fl/fl}$ *Cd4*^{Cre} *versus Tfam*$^{fl/fl}$ mice (n = 8-11, 5-month-old mice). (**G**) Time course (left) and representation of energy expenditure (right) during the dark period over a 24 hour cycle obtained using metabolic cages (n = 7-9). (**H**) Serum immunoglobulin titers against self-antigens at the age of 3, 7, and 22 months (n = 4-10). Anti-nuclear antibodies (ANAs), left; Extractable Nuclear Antigen antibodies (ENAs), right. Dots in all panels represent individual sample data. Data are presented as means ± SEM. Statistical analysis was by unpaired Student's *t* test [**A**, **B** (*mt16S*), **E** (IL-6, 3 months)**, F** (PLT, WBC) and **G**], unpaired Welch's *t*-test [**B** (*mtCo1* and *mtNd1*), **C** to **E** (IL-6, 5 months), **F** (RDWs and Granulocytes) and **H** (ANA 22 months)] or nonparametric Mann–Whitney *U* test [**H** (ANA 3, 7 months and ENA 3, 7, 22 months)]. *p<0.05, **p<0.01, ***p<0.001, ****p<0.0001.

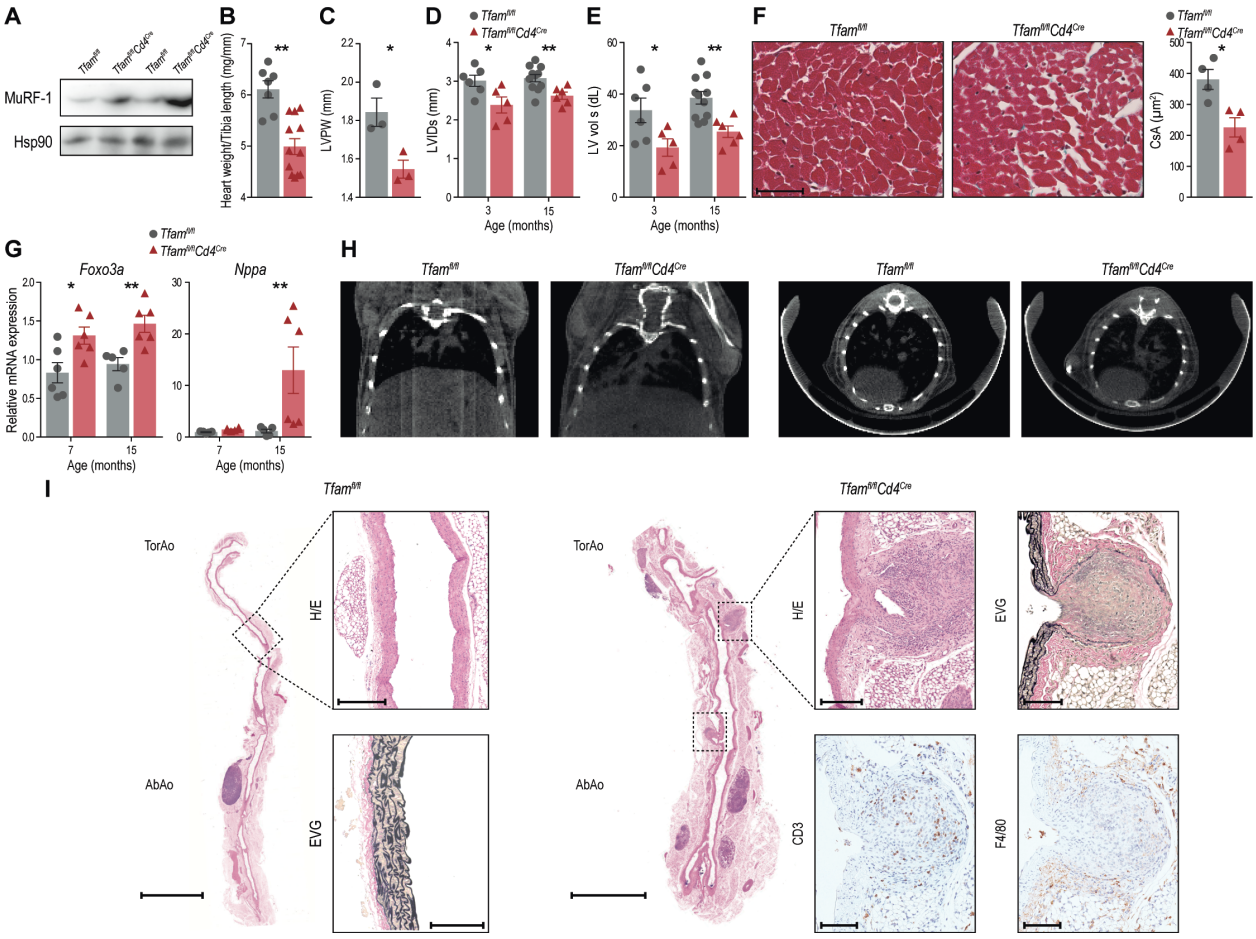
A
MuRF-1
Hsp90
B
Heart weight/Tibia length (mg/mm)
C
LVPW (mm)
D
LVIDs (mm)
Age (months)
E
LV vol s (dL)
Age (months)
F
CsA (μm²)
G
Foxo3a
Nppa
Relative mRNA expression
Age (months)
H
I
TorAo
AbAo
H/E
EVG
CD3
F4/80

Fig. S2

Fig. S2. *Tfam*$^{fl/fl}$ *Cd4*^{Cre} mice develop sarcopenia, heart failure and severe cardiovascular alterations.

(**A**) Western blot of MuRF-1 in tibialis from *Tfam*$^{fl/fl}$ and *Tfam*$^{fl/fl}$ *Cd4*^{Cre} mice. (**B**) Heart weight normalized to tibia length in *Tfam*$^{fl/fl}$ and *Tfam*$^{fl/fl}$ *Cd4*^{Cre} mice (n = 7-12 per group, 15-month-old). (**C**) Quantification of left ventricular posterior wall thickness (LVPW) by histological analysis of the heart from 15-month-old *Tfam*$^{fl/fl}$ and *Tfam*$^{fl/fl}$ *Cd4*^{Cre} mice (n = 3). (**D**) Echocardiography measurement of left ventricular internal diameter in systole (LVIDs) in 3- and 15-month-old *Tfam*$^{fl/fl}$ and *Tfam*$^{fl/fl}$ *Cd4*^{Cre} mice (n = 6-11). (**E**) Echocardiography measurement of left ventricular end-systolic volume (LV vol s) in 3- and 15-month-old *Tfam*$^{fl/fl}$ and *Tfam*$^{fl/fl}$ *Cd4*^{Cre} mice (n = 5-11). (**F**) Representative heart sections (left) and quantification of cardiomyocyte cross-sectional area (right) in 7-month-old *Tfam*$^{fl/fl}$ and *Tfam*$^{fl/fl}$ *Cd4*^{Cre} mice (n = 4 per group). Scale bar: 50 µm. (**G**) qPCR analysis of relative mRNA expression of *Foxo3a* (left) and *Nppa* (right) in heart extracts from 7- and 15-month-old *Tfam*$^{fl/fl}$ and *Tfam*$^{fl/fl}$ *Cd4*^{Cre} mice (n = 5-6). (**H**) Representative coronal section (left) and transversal section (right) acquired by CT scan from 4-month-old *Tfam*$^{fl/fl}$ and *Tfam*$^{fl/fl}$ *Cd4*^{Cre} mice (n = 5). (**I**) Representative H&E and elastic van Gieson (EVG) staining, together with immunostaining for CD3 (T cell marker) and F480 (macrophage marker) on aortic sections from 15-month-old *Tfam*$^{fl/fl}$ and *Tfam*$^{fl/fl}$ *Cd4*^{Cre} mice. Scale bar: 5 mm, 250 µm and 100 µm. Dots in all panels represent individual sample data. Data are presented as means ± SEM. Statistical analysis was by Student's *t* test [**C** to **E** and **G** (*Foxo3a* 7, 15 months and *Nppa* 7 months)] or nonparametric Mann–Whitney *U* test [**B**, **F** and **G** (*Nppa* 15 months)]. *p<0.05, **p<0.01, ***p<0.001, ****p<0.0001.

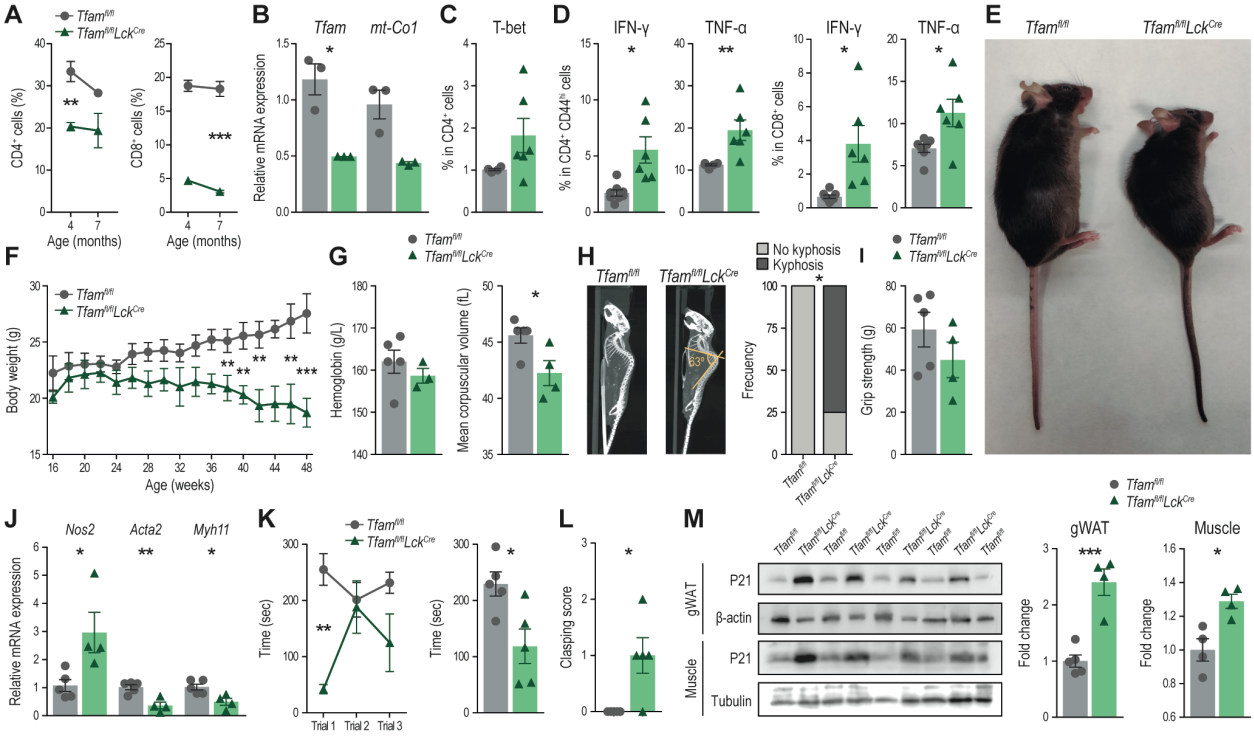
A
B
C
D
E
F
G
H
I
J
K
L
M
Tfam
mt-Co1
T-bet
IFN-γ
TNF-α
Age (months)
Age (weeks)
Body weight (g)
Hemoglobin (g/L)
Mean corpuscular volume (fL)
No kyphosis
Kyphosis
Frecuency
Grip strength (g)
Nos2
Acta2
Myh11
Relative mRNA expression
Time (sec)
Trial 1
Trial 2
Trial 3
Clasping score
P21
β-actin
Tubulin
gWAT
Muscle
Fold change

Fig. S3

Fig. S3. *Tfam*$^{fl/fl}$ *Lck*^{Cre} mice develop premature age-related multimorbidity.

(**A**) Frequencies of CD4$^+$ (left) and CD8$^+$ (right) were longitudinally measured in whole blood at 4 and 7-month-old *Tfam*$^{fl/fl}$ and *Tfam*$^{fl/fl}$ *Lck*^{Cre} (n = 4-5 per group). (**B**) *Tfam* and *mtCo1* mRNA levels in peripheral blood CD4$^+$ T cells from *Tfam*$^{fl/fl}$ and *Tfam*$^{fl/fl}$ *Lck*^{Cre} mice, (n = 3-4 per group). (**C**) T-bet intracellular expression in CD4$^+$ T cells in *Tfam*$^{fl/fl}$ and *Tfam*$^{fl/fl}$ *Lck*^{Cre} mice (n = 4-6 per group). (**D**) Quantification of intracellular cytokines IFN-γ and TNF-α in CD4$^+$ T cells (left) and CD8$^+$ T cells (right) in both mice groups (n = 6-7 per group). (**E**) Representative photograph showing the deteriorated physical appearance of 7-month-old *Tfam*$^{fl/fl}$ *Lck*^{Cre} mouse (right) compared with a control littermate (left). (**F**) Weight monitorization of *Tfam*$^{fl/fl}$ and *Tfam*$^{fl/fl}$ *Lck*^{Cre} mice. (**G**) Hemoglobin and MCV values from *Tfam*$^{fl/fl}$ and *Tfam*$^{fl/fl}$ *Lck*^{Cre} mice (n = 3-5). (**H**) Computed tomography (CT) scans (left) and percentage of mice presenting lordokyphosis (right) in *Tfam*$^{fl/fl}$ and *Tfam*$^{fl/fl}$ *Lck*^{Cre} mice (n = 4-5 per group, 10 months old). (**I**) Quantification of grip strength (n = 4-5, 10 months old). (**J**) qPCR analysis of *Nos2*, *Acta 2* and *Myh11* from aortic samples of *Tfam*$^{fl/fl}$ and *Tfam*$^{fl/fl}$ *Lck*^{Cre} mice (n = 4-5, 10 months old). (**K**) Performance in the rotarod test of *Tfam*$^{fl/fl}$ and *Tfam*$^{fl/fl}$ *Lck*^{Cre} mice expressed as the mean time spent in the rotating rod on each of three trials (left) or the total mean time (right) (n = 5, 10 months old mice). (**L**) Maximum clasping score per 30-s test (n = 4-5 per group, 10 months old mice). (**M**) Immunoblot (left) and protein fold change quantification (right) for p21 for gWAT and tibialis muscle (n = 4-5 per group, 10 months old mice). Dots in all panels represent individual sample data. Data are presented as means ± SEM. Statistical analysis was by Student's *t* test [**A**, **B**, **F**, **G** (hemoglobin), **H** to **K** and **M**], unpaired Welch's *t*-test [**C** and **D** (IFN-γ in CD4$^+$ T cells, IFN-γ and TNF-α in CD8$^+$ T cells)**]** or nonparametric Mann–Whitney *U* test [**D** (TNF-α in CD4$^+$ T cells), **G** (MCV) and **L**]. *p<0.05, **p<0.01, ***p<0.001, ****p<0.0001

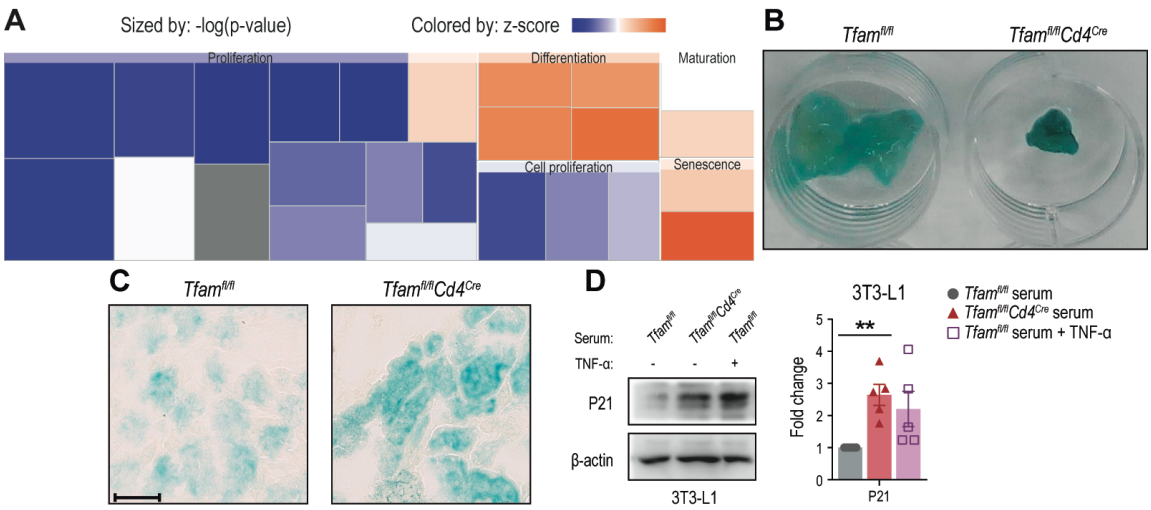
A
Sized by: -log(p-value)
Colored by: z-score
Proliferation
Differentiation
Maturation
Cell proliferation
Senescence
B
Tfam fl/fl
Tfam fl/fl Cd4 Cre
C
Tfam fl/fl
Tfam fl/fl Cd4 Cre
D
Serum:
TNF-α:
P21
β-actin
3T3-L1
3T3-L1
Tfam fl/fl serum
Tfam fl/fl Cd4 Cre serum
Tfam fl/fl serum + TNF-α
Fold change
P21
**

Fig. S4

Fig. S4. Premature senescence in *Tfam*$^{fl/fl}$ *Cd4*^{Cre} mice.

(A) IPA heatmap showing transcriptionally dysregulated cellular pathways in *Tfam*$^{fl/fl}$ *Cd4*^{Cre} mice (n = 3-4 animals per group, 7 months old). The heatmap is sized by –log (p-value) and colored by z-score. **(B)** β-galactosidase activity staining in collected gWAT depots. **(C)** Representative images of β-gal staining in kidney cryosections. Scale bar: 50 μm. **(D)** Immunoblot (left) and densitometry analysis (right) of 3T3-L1 cells cultured in the presence of *Tfam*$^{fl/fl}$ or *Tfam*$^{fl/fl}$ *Cd4*^{Cre} serum or *Tfam*$^{fl/fl}$ serum supplemented with recombinant TNF-α. Blots are representative of five experiments using pooled sera from three animals. Dots in all panels represent individual sample data. Data are presented as means ± SEM. Statistical analysis was by one-way analysis of Kruskal–Wallis *H* test with post hoc Dunn´s correction [**D**]. *p<0.05, **p<0.01, ***p<0.001, ****p<0.0001.

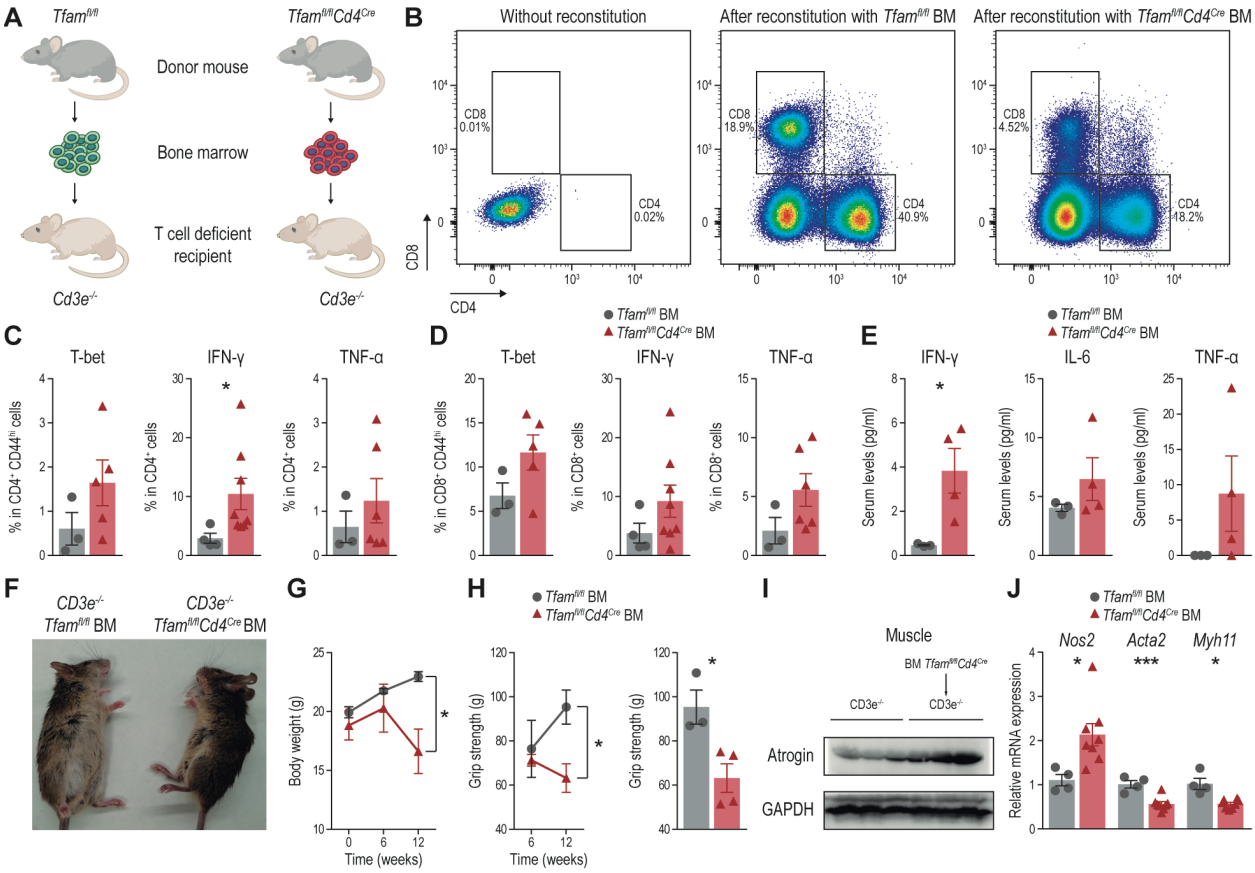
A
Tfam^fl/fl
Tfam^fl/flCd4^Cre
Donor mouse
Bone marrow
T cell deficient recipient
Cd3e^-/-
Cd3e^-/-
B
Without reconstitution
After reconstitution with Tfam^fl/fl BM
After reconstitution with Tfam^fl/flCd4^Cre BM
CD8
CD4
CD8 0.01%
CD4 0.02%
CD8 18.9%
CD4 40.9%
CD8 4.52%
CD4 18.2%
C
T-bet
IFN-γ
TNF-α
% in CD4+ CD44hi cells
% in CD4+ cells
D
Tfam^fl/fl BM
Tfam^fl/flCd4^Cre BM
T-bet
IFN-γ
TNF-α
% in CD8- CD44hi cells
% in CD8+ cells
E
Tfam^fl/fl BM
Tfam^fl/flCd4^Cre BM
IFN-γ
IL-6
TNF-α
Serum levels (pg/ml)
F
CD3e^-/- Tfam^fl/fl BM
CD3e^-/- Tfam^fl/flCd4^Cre BM
G
Body weight (g)
Time (weeks)
H
Tfam^fl/fl BM
Tfam^fl/flCd4^Cre BM
Grip strength (g)
Time (weeks)
I
Muscle
BM Tfam^fl/flCd4^Cre
CD3e^-/-
CD3e^-/-
Atrogin
GAPDH
J
Tfam^fl/fl BM
Tfam^fl/flCd4^Cre BM
Nos2
Acta2
Myh11
Relative mRNA expression

Fig. S5

Fig. S5. Transfer of *Tfam*$^{fl/fl}$ *Cd4*^{Cre} bone marrow recapitulates the aging phenotype in recipient mice.

(**A**) BM precursors from *Tfam*$^{fl/fl}$ *Cd4*^{Cre} and *Tfam*$^{fl/fl}$ mice were injected i.v. into T cell deficient *Cd3e*$^{-/-}$ mice. (**B**) Data shown are representative flow cytometry plots of lymph node CD4^{+} and CD8^{+} cells in *Cd3e*$^{-/-}$ without reconstitution (left) or reconstitution with bone marrow (BM) precursors from *Tfam*$^{fl/fl}$ (center) or *Tfam*$^{fl/fl}$ *Cd4*^{Cre} mice (right). (**C**) Percentages of CD4^{+} cells positive for T-bet, IFN-γ, and TNF-α (n = 3-8). (**D**) Percentages of CD8^{+} cells positive for T-bet, IFN-γ, and TNF-α (n = 3-8). (**E**) Multiplex detection of circulating cytokines in *Cd3e*$^{-/-}$ chimeras 16 weeks after BM transplant with *Tfam*$^{fl/fl}$ *Cd4*^{Cre} or without reconstitution (n = 3-4 per group). (**F**) Representative photograph of *Cd3e*$^{-/-}$ chimeras 16 weeks after transplantation. (**G**) Body weight evolution of *Cd3e*$^{-/-}$ chimeras after transplantation (n = 3-4 per group). (**H**) Time course evolution of forelimb strength after BM transplant (left), quantification of grip strength 12 weeks after the transplant (right) (n = 3-4 per group). (**I**) Expression of Atrogin-1 in tibialis from *Cd3e*$^{-/-}$ transferred with BM from *Tfam*$^{fl/fl}$ *Cd4*^{Cre}. GAPDH was used as loading control (n = 3-4 per group). (**J**) qPCR analysis of *Nos2*, *Acta2*, and *Myh11* mRNA expression levels in aorta from *Cd3e*$^{-/-}$ transferred with BM from *Tfam*$^{fl/fl}$ *Cd4*^{Cre} or *Tfam*$^{fl/fl}$ mice (n = 4-8). Dots in all panels represent individual sample data. Data are presented as means ± SEM. Statistical analysis was by two-way ANOVA with correction for multiple comparisons by post hoc Sidak's test [**G** and **H** (monitorization)], Student's *t* test [**C** (T-bet and TNF-α in CD4^{+}), **D**, **H**, and **J** (*Nos2* and *Acta2*)], unpaired Welch's *t*-test [**E** (IFN-γ and IL-6) and **J** (*Myh11*)] or nonparametric Mann–Whitney *U* test [**C** (IFN-γ in CD4^{+}) and **E** (TNF-α)]. *p<0.05, **p<0.01, ***p<0.001, ****p<0.0001.

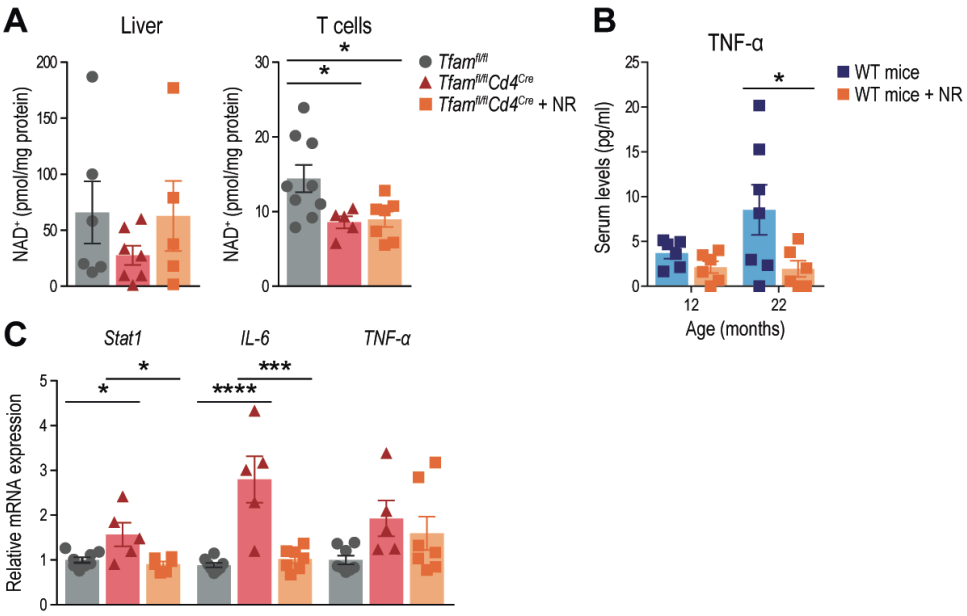
A
Liver
T cells
NAD+ (pmol/mg protein)
Tfam fl/fl
Tfam fl/fl Cd4 Cre
Tfam fl/fl Cd4 Cre + NR
B
TNF-α
Serum levels (pg/ml)
WT mice
WT mice + NR
Age (months)
C
Stat1
IL-6
TNF-α
Relative mRNA expression

Fig. S6

Fig. S6. Effects of NR in *Tfam*$^{fl/fl}$ *Cd4*^{Cre} mice and old wt mice.

(A) NAD^+ levels in liver (left) and $CD4^+$ T cells (right) lysates from *Tfam*$^{fl/fl}$, *Tfam*$^{fl/fl}$ *Cd4*^{Cre} and NR-treated *Tfam*$^{fl/fl}$ *Cd4*^{Cre} mice (n = 5-9 per group). (**B**) TNF-α serum levels in 12- and 22-month-old wt mice treated over 10 weeks with saline (control) or NR. (n = 6-7 per group). (**C**) mRNA expression of *Stat1, Il-6* and *Tnf-α* in the liver (n = 5-8) of *Tfam*$^{fl/fl}$, *Tfam*$^{fl/fl}$ *Cd4*^{Cre} and NR-treated *Tfam*$^{fl/fl}$ *Cd4*^{Cre} mice. Dots in all panels represent individual sample data. Data are presented as means ± SEM. Statistical analysis was by one-way analysis of variance (ANOVA) with post hoc Turkey´s correction [**A**, **B** and **C** (*Stat1* and *Il-6*)] or Kruskal–Wallis *H* test with post hoc Dunn´s correction [**C** (*Tnf-α*)]. *p<0.05, **p<0.01, ***p<0.001, ****p<0.0001.

Other Supplementary Material for this manuscript includes the following:

Table S1 (Microsoft Excel format). IPA analysis of liver transcriptomics to identify upstream regulators potentially driving transcriptional changes between *Tfam*$^{fl/fl}$ *Cd4*^{Cre} mice untreated or treated with NR.